

ENCLOSURE 2

MFN 10-358

NEDO-33353, Revision 0
Application of GNF-Ziron to GNF Fuel Designs
December 2010

Non-Proprietary Information – Class I (Public)

IMPORTANT NOTICE

This is a non-proprietary version of NEDC-33353P, Revision 0, which has the proprietary information removed. Portions of the document that have been removed are indicated by white space with an open and closed bracket as shown here [[]].



Global Nuclear Fuel

A Joint Venture of GE, Toshiba, & Hitachi

Global Nuclear Fuel

NEDO-33353
Revision 0
DRF Section 0000-0127-4981 R0
December 2010

Non-Proprietary Information – Class I (Public)

Licensing Topical Report

**Application of GNF-Ziron
to
GNF Fuel Designs**

Copyright 2010 Global Nuclear Fuel – Americas, LLC

All Rights Reserved

INFORMATION NOTICE

This is a non-proprietary version of the document NEDC-33353P, Revision 0, which has the proprietary information removed. Portions of the document that have been removed are indicated by an open and closed bracket as shown here [[]].

IMPORTANT NOTICE REGARDING CONTENTS OF THIS REPORT

PLEASE READ CAREFULLY

The design, engineering, and other information contained in this document is furnished for the purpose of supporting the NRC review and approval of the GNF-Ziron Licensing Topical Report. The only undertakings of GNF-A with respect to information in this document are contained in the contracts between GNF-A and its customers or participating utilities, and nothing contained in this document shall be construed as changing that contract. The use of this information by anyone for any purpose other than that for which it is intended is not authorized; and with respect to any unauthorized use, GNF-A makes no representation or warranty, and assumes no liability as to the completeness, accuracy, or usefulness of the information contained in this document.

TABLE OF CONTENTS

Section	Title	Page
1.0	Introduction.....	1-1
2.0	GNF-Ziron Characteristics and Experience.....	2-1
2.1	GNF-Ziron Characteristics.....	2-1
2.2	Testing & Operating Experience	2-2
2.3	Benefit of GNF-Ziron: Hydrogen Absorption	2-2
2.4	Benefit of GNF-Ziron: Corrosion	2-5
2.4.1	Corrosion of GNF-Ziron: General Corrosion	2-6
2.4.2	Corrosion Benefit of GNF-Ziron: Under Enhanced Corrosion Conditions.....	2-7
3.0	Methods and Licensing Assessment	3-1
3.1	Fuel Design Licensing	3-1
3.2	Nuclear & Thermal/Hydraulic Methods	3-1
3.3	Thermal/Mechanical Methods	3-2
3.3.1	Fuel Rod Internal Pressure.....	3-3
3.3.2	Fuel Melting.....	3-4
3.3.3	Cladding Strain	3-4
3.3.4	Cladding Stress/Strain.....	3-5
3.3.5	Cladding Fatigue.....	3-5
3.3.6	Cladding Creep Collapse	3-6
3.3.7	Postulated Loss-of-Coolant Accident	3-6
3.3.8	Reactivity Insertion Accident	3-8
4.0	Mechanical Design Assessment.....	4-1
5.0	Summary	5-1
6.0	References.....	6-1
A.	GNF-Ziron Metallurgical Characteristics.....	A-1
A.1	GNF-Ziron Composition.....	A-1
A.2	Material Processing.....	A-2
A.3	Basic Metallurgical Characteristics	A-3
A.3.a	Grain Structure and Size	A-3
A.3.b	Texture	A-4
A.3.c	Second Phase Particles.....	A-5

B.	Material Properties Assessment Physical Properties	A-1
B.1	Physical Properties.....	B-1
B.1.a	Metal Properties	B-1
B.1.b	Oxide Properties.....	B-1
B.2	Thermal Properties.....	B-1
B.2.a	Oxide Properties.....	B-3
B.3	Mechanical Properties.....	B-4
B.3.a	Modulus and Poisson’s Ratio.....	B-4
B.3.b	Tensile Properties.....	B-4
B.3.c	Perforation Stress	B-10
B.3.d	Hardness.....	B-11
B.3.e	Fatigue.....	B-11
B.3.f	Creep.....	B-12
B.4	Irradiation Growth	B-14
B.5	High Temperature Behavior	B-17
B.5.a	High Temperature Oxidation Kinetics.....	B-17
B.5.b	Post-Quench Ductility.....	B-18
C.	References for Appendices	C-1

LIST OF TABLES

Table	Title	Page
Table 2-1	Summary of Corrosion Oxide Thickness Test Results Performed in the BWR Corrosion Loop of the Halden Test Reactor	2-10
Table 3-1	Fuel Rod Thermal-Mechanical Design Criteria.....	3-10
Table 4-1	Considerations for Supplementary Zircaloy Mechanical Design Bases	4-2
Table A-1	GNF Alloy Chemical Composition for GNF-Ziron and Zircaloy	A-2
Table A-2	Comparison of Outer Surface SPP Size in GNF-Ziron and Zircaloy-2 Cladding [[]]	A-7
Table B-1	Thermal Properties of GNF-Ziron Unaffected by Composition Difference Between GNF-Ziron and Zircaloy	B-2

LIST OF FIGURES

Figure	Title	Page
Figure 2-1	In-Reactor Operational Experience of GNF-Ziron.....	2-11
Figure 2-2	Hydrogen Content as a Function of Accumulated Fast Neutron Fluence.....	2-12
Figure 2-3	Corrosion Weight Gain as a Function of Accumulated Fast Neutron Fluence.....	2-13
Figure 2-4	Hydrogen Concentration as a Function of Corrosion Weight Gain.....	2-14
Figure 2-5	Hydrogen Pickup as a Function of Accumulated Fast Neutron Fluence.....	2-15
Figure 2-6	Hydrogen Concentration in Water Rods and Unfueled Cladding as a Function of Residence Time	2-16
Figure 2-7	Hydrogen Concentration in Fuel Cladding as a Function of Residence Time.....	2-17
Figure 2-8	Channel Shadow Corrosion Bow After 1 and 2 Cycles of Operation.....	2-18
Figure 2-9	Corrosion Weight Gain After 72 Hours Autoclave Testing at 400°C For Zircaloy-2 and GNF-Ziron as a Function of [[]].....	2-19
Figure 2-10	Corrosion Weight Gain After Two-Step Test at 410°C /520°C for Zircaloy-2 and GNF-Ziron as a Function of [[]].....	2-20
Figure 2-11	Poolside Eddy Current Liftoff from LUA Programs at Plant G And Plant V	2-21
Figure 2-12	Comparison Of Visual Appearances of GNF-Ziron (Lower Row) And Zircaloy-2 (Upper Row) Cladding Away from Spacer Locations after [[]] Exposure (Plant G).....	2-22
Figure 2-13	Comparison of Visual Appearances of GNF-Ziron (Lower Row) And Zircaloy-2 (Upper Row) Cladding Away from Spacer Locations after [[]] Exposure (Plant V).....	2-23
Figure 2-14	Metallographic Oxide Thickness in GNF-Ziron And Zircaloy-2 Water Rods after [[]] Bundle Average Exposure (Plant G).....	2-24
Figure 2-15	Comparison of Visual Appearances of GNF-Ziron (Lower Row) and Zircaloy-2 (Upper Row) Cladding at Spacer Locations at Similar Axial Elevations after [[]] Bundle Average Exposure (Plant G).....	2-25

Figure 2-16	Visual Appearance Water Rod Made from GNF-Ziron (Right and Zircaloy-2 (Left) at a Spacer Location (~36 Inch Elevation) after [[]] Bundle Average Exposure (Plant G).....	2-26
Figure 2-17	Comparison of Eddy Current Liftoff Measurements at Spacer Locations.....	2-27
Figure 2-18	Comparison of Visual Appearances of GNF-Ziron (Lower Row) and Zircaloy-2 (Upper Row) Cladding at Spacer Locations at Same Axial Elevation after ~15 GWd/MTU Exposure (Plant V)	2-28
Figure A-1	Examples of [[]] in Cladding of Ziron (left) and Zircaloy-2 (right).....	A-4
Figure A-2	Comparison of Texture in GNF-Ziron and Zircaloy-2 10x10 Cladding (Upper) and Channel Strip (Lower)	A-5
Figure A-3	TEM Micrograph Showing SPPs in [[]].....	A-8
Figure A-4	Changes in Fe Content in $Zr(Fe,Cr)_2$ and $Zr_2(Fe,Ni)$ SPPs in GNF-Ziron and Zircaloy-2	A-9
Figure B-1	Comparison of Thermal Conductivity of GNF-Ziron with Reference Zircaloy-2 as a Function of Temperature	B-3
Figure B-2	Yield Strength, Ultimate Tensile Strength and Elongation at Room Temperature and at 343°C Elevated Temperature for GNF-Ziron and Zircaloy-2.....	B-6
Figure B-3	Yield Strength as a Function of Fluence at Room and Elevated Temperatures.....	B-7
Figure B-4	Ultimate Tensile Strength as a Function of Fluence at Room and Elevated Temperatures.....	B-8
Figure B-5	Total Elongation as a Function of Fluence at Room and Elevated Temperatures.....	B-9
Figure B-6	High Temperature Burst Test Data for GNF-Ziron Compared with Zircaloy Correlation Lines for Different Heating Rates (Reference 3).....	B-10
Figure B-7	Hardness as a Function of Fluence	B-11
Figure B-8	Cyclic Strain Amplitude as a Function of Cycles.....	B-12
Figure B-9	Creep Strain of GNF-Ziron and Zircaloy-2 as a Function of Fast Fluence.....	B-13
Figure B-10	Adjusted Creep Strain as a Function of Fluence for GNF-Ziron and Zircaloy-2.....	B-14
Figure B-12	Comparison of Water Rod Growth of GNF-Ziron with Zircaloy-2	B-17

Figure B-13	Comparison of Weight Gain for GNF-Ziron and Zircaloy-2 at 1000°C.....	B-19
Figure B-14	Comparison of Weight Gain for GNF-Ziron and Zircaloy-2 at 1200°C.....	B-20
Figure B-15	Comparison of Weight Gain for GNF-Ziron at 1000°C with Baker-Just and Cathcart-Pawel Relationships.....	B-21
Figure B-16	Post-Quench Ductility (Offset Strain) at Room Temperature for GNF-Ziron and Zircaloy-2 as a Function of ECR at 1000°C Followed by Quench from 800°C.....	B-22
Figure B-17	Post-Quench Ductility (Offset Strain) at 135°C for GNF-Ziron and Zircaloy-2 as a Function of ECR at 1200°C Followed by Quench from 800°C.....	B-23
Figure B-18	Post-Quench Ductility (Permanent Strain) at Room Temperature for GNF-Ziron and Zircaloy-2 as a Function of ECR at 1000°C Followed by Quench from 800°C.....	B-24
Figure B-19	Post-Quench Ductility (Permanent Strain) at 135°C for GNF-Ziron and Zircaloy-2 as a Function of ECR at 1200°C Followed by Quench from 800°C.....	B-25

ACRONYMS AND ABBREVIATIONS

Term	Definition
ANL	Argonne National Laboratory
AOO	Anticipated Operational Occurrence
ASTM	American Society for Testing and Materials
ATR	Advanced Test Reactor
BJ	Baker-Just
BWR	Boiling Water Reactor
CG	Control Group
CG1	Control Group 1
CG2	Control Group 2
CP	Cathcart-Pawel
Cr	Chromium
CRDA	Control Rod Drop Accident
EC	Eddy Current
ECCS	Emergency Core Cooling System
ECR	Equivalent Cladding Reacted
ET	Elevated Temperature
Fe	Iron
GESTAR	General Electric Standard Application for Reactor Fuel
GNF	Global Nuclear Fuel – Americas, LLC
GWd/MTU	Gigawatt Days per Metric Ton of Uranium
ID	Inside Diameter
IPHT	In-Process Heat Treatment
LHGR	Linear Heat Generation Rate
LOCA	Loss-of-Coolant Accident
LUA	Lead Use Assembly
MELO	Maximum Effective Liftoff
Ni	Nickel
NRC	United States Nuclear Regulatory Commission
O	Oxygen
OD	Outside Diameter
PPE	Peak Pellet Exposure
ppm	Parts per million
RIA	Reactivity Insertion Accident
RT	Room Temperature
Sn	Tin
SPP	Second Phase Particles
TEM	Transmission Electron Microscope
US	United States

Term	Definition
UTS	Ultimate Tensile Strength
YS	Yield Strength
Zr	Zirconium

EXECUTIVE SUMMARY

This document provides the technical justification to apply GNF-Ziron, a zirconium alloy with composition modified from that of Zircaloy-2, which Global Nuclear Fuel - Americas, LLC (GNF) currently utilizes in GNF fuel designs for fuel rods, spacers and water rods. GNF has performed testing and analyses to determine that GNF-Ziron is equivalent, or superior, to Zircaloy-2 with respect to physical requirements, thermal-mechanical performance criteria, as well as other operational performance criteria such as corrosion resistance and hydrogen absorption for application within specified GNF fuel assembly components.

REVISIONS

Rev	Purpose of Revision	Reference
0	Initial Issue	--

1.0 Introduction

Global Nuclear Fuel – Americas, LLC (GNF) has developed a zirconium alloy, designated as GNF-Ziron, with demonstrated capability to meet application requirements of components in GNF fuel designs. The primary reason for developing this alloy has been the general trend of the nuclear industry towards higher exposures and the desire to decrease the effect this may have on performance and safety compliance for GNF fuel designs. As such, the focus of this development program has been to identify an alloy with thermal and mechanical properties equal to or exceeding those of Zircaloy-2, while improving the resistance of fuel components to in-service degradation effects, in particular the effects due to absorbed corrosion-generated hydrogen.

Currently, Zircaloy-2 is the zirconium alloy of choice for fuel assembly components in licensed GNF fuel designs which includes fuel rod cladding, water rods, fuel spacers (also termed as spacer grids or grid-spacers), channels and end plugs. For cladding, water rods, fuel spacers and end plugs, Zircaloy-2 has been licensed as a fuel assembly material. For channels, Zircaloy-2 and Zircaloy-4 has been licensed. GNF has performed testing and analysis with GNF-Ziron and has determined the performance of GNF-Ziron to be [[]] and therefore an acceptable material for use as a fuel assembly material. [[]]

This document demonstrates that material performance of GNF-Ziron meets relevant design bases for application to GNF fuel [[]]

[[]] Section 2.0 and Appendices A and B summarize the metallurgical characteristics, the properties and the experience base for GNF-Ziron. Section 2.0 includes a discussion of anticipated conditions, [[]]

[[]] Section 3.0 addresses application of GNF-Ziron within GNF fuel licensing bases, with technical assessment of the effect of GNF-Ziron on approved methods, including the regulatory requirements covered specifically by the licensed methods and requirements of 10 CFR Part 50. In Section 4.0, GNF’s mechanical design criteria are reviewed to evaluate the anticipated effect on fuel bundle mechanical designs from deployment of GNF-Ziron rather than Zircaloy-2 (or Zircaloy-4) as the fuel component material.

GNF licenses fuel designs with the Nuclear Regulatory Commission (NRC) based on specific analyses performed in accordance with the fuel licensing acceptance criteria as specified in General Electric Standard Application for Reactor Fuel (GESTAR) II (Reference 1.1) (often referred to as the “Amendment 22” process). This document summarizes the performance of GNF-Ziron, demonstrating that GNF-Ziron complies with approved methods and is capable of performing acceptably in a boiling water reactor (BWR). Compliance to approved methods will be demonstrated by evaluating alloying characteristics, as well as in-reactor and test data obtained for GNF-Ziron, [[]]

[[]] Upon NRC approval of GNF-Ziron, GNF will revise and submit the

Amendment 22 compliance reports to incorporate GNF-Ziron material within applicable GNF fuel products.

2.0 GNF-Ziron Characteristics and Experience

2.1 GNF-Ziron Characteristics

GNF-Ziron (previously described as High-Fe Zircaloy-2) is the outcome of many years of research for an improved material for cladding and fuel assembly components in GNF fuel products. The primary objective of this research has been to identify an alloy with good corrosion resistance and reduced hydriding characteristics.

The chemical composition of GNF-Ziron is an evolution from that of Zircaloy-2. GNF-Ziron has a [[]], which is based on a nominal composition of [[]] manufacturing tolerance. The concentrations of other elements [[]]

[[]] Like Zircaloy-2 currently used by GNF, GNF-Ziron is manufactured from sponge zirconium produced from the Kroll process. GNF plans to use the same manufacturing process to produce GNF-Ziron cladding and fuel assembly components as has been used for Zircaloy-2; though some details of these fabrication processes may change or evolve with time as was true for Zircaloy-2 cladding and components. (See Appendix A for more detailed description regarding fabrication.)

Because the [[]] and the same manufacturing process is used, the [[]]
[[]] Consequently, there is [[]], because such properties are more dependent on changes in [[]] changes. (Appendix A.)

The second phase particles (SPPs) in GNF-Ziron [[]]
[[]] The composition change relative to Zircaloy-2 results in a difference in the composition and number density of the SPPs in GNF-Ziron (Appendix A). These changes are [[]]
[[]] (Appendix B), but, in principle, may affect the corrosion behavior. However, observations from in-reactor operation have [[]]
[[]] between GNF-Ziron and Zircaloy-2, although there are several indications that show [[]]
[[]] for GNF-Ziron [[]]. The corrosion behavior of GNF-Ziron, compared with Zircaloy-2, is discussed further in Section 2.4. The [[]]
[[]], as discussed in Section 2.3. [[]]
[[]] The available information thus suggests that the [[]]

[[]] that provides the [[]]

]]

2.2 Testing & Operating Experience

Following laboratory testing during the 1980's, GNF-Ziron has been exposed to a number of in-reactor evaluations including the Advanced Test Reactor (ATR), Plant C in the United States (US), the Halden test reactor in Norway, Plant K in Japan, and the BOR-60 test reactor in Russia. As summarized in Figure 2-1, the general corrosion behavior was first evaluated in Plant C, followed by irradiation at Halden with a variety of water chemistry conditions. The corrosion and hydriding characteristics were further assessed in Plant K. The Plant K program included an extensive assessment of the mechanical properties and microstructural evolution of unfueled cladding manufactured from GNF-Ziron. The irradiation programs at ATR and BOR-60 addressed the irradiation growth behavior for GNF-Ziron. The performance of this alloy under simulated accident conditions has also been assessed in Japan and at Argonne National Laboratory (ANL). Lead Use Assemblies (LUAs) consisting of [[

]] manufactured from GNF-Ziron were irradiated in Plant G in Europe starting in 1999, reaching [[]] bundle-averaged exposures in October of 2005. LUA performance was assessed periodically during operation using poolside inspection. Following discharge in 2005, selected rods were sent to a hot cell for more detailed evaluation. In a continuation of this LUA program, [[]] of the GNF-Ziron assemblies have been reinserted in 2008 for two additional years of operation.

More recently, LUAs with GNF-Ziron cladding were inserted into Plant V in the summer of 2007 and have completed 2 cycles of operation. Other LUAs with GNF-Ziron are currently operating at Plant F (initiated in the summer of 2008) and Plant H (initiated in the spring of 2009). Plant H will be introducing a second LUA program starting in 2011. Additionally, channels manufactured from GNF-Ziron have completed [[]] 24-month cycles of operation at Plant P (started in Spring 2005) and at Plant N (started in Spring 2006) in the US. The results from the testing and LUA programs are discussed in relevant portions of this document and also in Appendices A and B.

2.3 Benefit of GNF-Ziron: Hydrogen Absorption

The corrosion behavior and associated hydrogen absorption of GNF-Ziron, relative to that of Zircaloy-2, is assessed from the irradiation program at Plant K. The program included the evaluation of unfueled GNF-Ziron and Zircaloy-2 cladding irradiated to high exposures using dummy neutron source holders in a commercial reactor. The evolution of hydrogen content in GNF-Ziron with fast neutron fluence is shown in Figure 2-2. The results show that, [[

]] After [[]] cycles of irradiation, at [[

]]

A similar trend with exposure is observed for corrosion weight gain, Figure 2-3. For [[

]] is evident from the hydrogen versus weight gain plot shown in Figure 2-4.

Figure 2-2 through Figure 2-4 collectively indicate that the hydrogen pickup [[
]], as shown in Figure 2-5. In Figure 2-5, GNF-Ziron also shows [[

]]
In Figure 2-2 to Figure 2-5, the [[
]] Zircaloy-2 samples covered the fast neutron fluence range of [[
]] while GNF-Ziron covered [[
]]). This range in fluence level [[
]] provides an insight into the behavior for Zircaloy-2. Figure 2-2 shows that at [[

]] of irradiation. The implication is that the [[

]] The data for Zircaloy-2 suggest that [[

]] The description for [[
]] is consistent with other observations reported in the literature (Reference 2.1). In summary, the irradiation program from Plant K [[

]]
GNF's experience with hydrogen content in water rods is consistent with the data from Plant K and [[
]] Figure 2-6 shows hydrogen content in Zircaloy-2 water rods together with data from the irradiation program at Plant K, which were based on non-fueled cladding. Figure 2-6 includes hydrogen data for GNF-Ziron and companion Zircaloy-2 water rods from the LUA program at Plant G. The water rod hydrogen data indicates [[

]] of operation, based on measurements taken from a water rod irradiated in a US plant. However, water rods after [[
]] at Plant G showed [[

]] A possible explanation is in the plant condition, such as water chemistry, between the reference US plant and Plant G in Europe, such

that [[

]]

The hydrogen contents [[

]] as a function of residence time is shown in Figure 2-7.

The data for Zircaloy-2 were obtained from different fuel designs involving different cladding thicknesses. Because absorbed hydrogen in cladding results from surface corrosion, the hydrogen concentration will be dependent on the cladding thickness. In order to compare the hydrogen content for the same cladding thickness, the hydrogen contents shown have been normalized [[

]] Compared with

Figure 2-6, the hydrogen content [[

]] This difference is consistent with [[

]]. As

with hydrogen in water rods, a [[

]] is evident.

Figure 2-7 provides a GNF-Ziron vs. Zircaloy-2 comparison of cladding from the LUA program at Plant G after [[

]] of irradiation. Hydrogen data were obtained from [[

GNF-Ziron fuel rods in [[

]] assemblies and from [[

]] Zircaloy-2 fuel rods from [[

]] assembly following discharge at [[

]] bundle average exposure.

Other Zircaloy-2 cladding data in the [[

]] operating time frame had bundle average

exposure ranging between [[

]] than the LUAs from

Plant G. Figure 2-7 shows that the cladding hydrogen levels after [[

]] irrespective of the exposure [[

]], and [[

]] The [[

]]

]] A [[

]] between GNF-Ziron and Zircaloy-2

cladding at [[

]]

Indirect comparison of the hydrogen pickup characteristics of GNF-Ziron relative to Zircaloy-2 has been obtained from the lead use channel program at Plant P. In this channel LUA program, [[

]] GNF-Ziron and Zircaloy-2 channels were operated within two distinct control groups (CGs) of symmetric bundles, where one control group (CG1) obtained significantly more early life exposure to the control blade than the second control group (CG2). After each of [[

]] cycles of operation, channel dimensions were measured on [[

]] GNF-Ziron channels as well as on the [[

]] control Zircaloy-2 channels that were operated in symmetric core locations and thus experienced the same control blade exposure and hence expected shadow corrosion. For each channel, the deflection or bow across two pairs of opposing channel faces was measured. From the measured data, the shadow corrosion induced channel bow is deduced by subtracting the calculated bow due to irradiation growth from the measured bow as shown in

Figure 2-8. Based on prior poolside measurements and hot cell investigations, shadow corrosion induced bow has been correlated to the hydrogen differential across the channel (Reference 2.2), and is thus an indicator of hydrogen absorption, as indicated by the alternate vertical scale in Figure 2-8. In both cases, GNF-Ziron channels [[

]] in Figure 2-8. For the other control group, CG1, GNF-Ziron and Zircaloy-2 developed [[

]] for Zircaloy-2 channels than GNF-Ziron channels, which [[

]] The [[]] for the Zircaloy-2 channels in CG1 is consistent with the recent investigation (Reference 2.3), which confirmed that the [[

]] is indicative of a reduced tendency to [[]]

The channel bow data in Figure 2-8 and the hydrogen absorption data from the K-5 irradiation program both support the conclusion that GNF-Ziron has [[

]]

2.4 Benefit of GNF-Ziron: Corrosion

The main difference in material characteristics resulting from the [[]] of SPPs.

SPPs in Zircaloys generally are known to affect the corrosion behavior. Therefore, in principle, a [[]]

Laboratory tests, supported by in-reactor performance, have shown that [[]] and appears to be sensitive to the testing condition. In

Figure 2-9, the corrosion weight gain data following American Society for Testing and Materials (ASTM) G2 corrosion testing (72 hr @ 400°C) is shown as a function of the [[

]] Figure 2-9 shows that [[]] under this industry standard test condition. A companion set of cladding

was tested under 1750 psi (12.1 MPa) pressure at 410°C followed by 520°C. This test condition is routinely used by GNF and is considered to be more severe than the ASTM G2 test and to be a more relevant indicator of nodular corrosion performance in BWRs. The weight gain results, Figure 2-10, show that there is [[]] in weight gain [[

]] It should be noted that all test samples shown in Figure 2-10 did not develop any nodules. The no-nodules performance means that the corrosion performances of Zircaloy-2 and GNF-Ziron are both very good, because no-nodule is the most

stringent visual criterion for the 410°C/520°C test, which was developed with correlation to corrosion performance in BWRs. The [[]] in the G2 test and the [[]] under the more severe 410°C/520°C test collectively indicate [[]] (i.e., [[]] for GNF-Ziron).

In-reactor corrosion performance of GNF-Ziron relative to Zircaloy-2 appears to be consistent with expectations based on the laboratory test results in Figure 2-10. The expectation is therefore for [[]] under typical BWR water chemistry conditions; [[]]

2.4.1 Corrosion of GNF-Ziron: General Corrosion

The general corrosion performance of GNF-Ziron under typical BWR conditions has been obtained from the irradiation program at Plant K and from LUA programs at Plant G and Plant V. The corrosion weight gain for GNF-Ziron and Zircaloy-2 as a function of fast neutron fluence from the Plant K program is shown in Figure 2-3. As noted earlier, [[]]

In the LUAs at Plant G and Plant V, poolside eddy current (EC) liftoff measurements, shown in Figure 2-11, for GNF-Ziron and companion Zircaloy-2 cladding are consistent with GNF's considerable experience base (which is not shown in Figure 2-11 for clarity). EC liftoff measures the gap distance between the EC probe and the base metal of the zirconium-based component. EC liftoff therefore measures the combined thickness of the corrosion layer as well as the crud layer that generally forms during in-reactor operation. The nature of the crud layer deposition, both thickness and microstructure, is strongly dependent on reactor water parameters such as the Fe and Zn concentrations as well as the local nodal power. Crud deposition is not influenced by cladding material. Because magnetic crud deposits can affect the EC measurement data, falsely indicating much thicker crud layers than actually deposited, the EC liftoff measurement data is corrected using conservative methods. In both cases, whether magnetic crud is detected or not, the EC liftoff measurements include crud deposition and therefore provide a conservative assessment of the cladding corrosion.

From the LUAs at Plant G, poolside inspections were performed on GNF-Ziron at various times up to [[]] bundle average exposure. At [[]], inspections were performed on both GNF-Ziron and Zircaloy-2. These inspection results showed GNF-Ziron performed as expected relative to GNF's experience base. The comparison at [[]] showed that the general corrosion characteristic for GNF-Ziron [[]] for Zircaloy-2. Representative pictures of cladding appearance at [[]] bundle average exposure are shown in Figure 2-12. Figure 2-12 shows the comparison at elevations away from spacer locations. (Enhanced corrosion or shadow corrosion at spacer locations is discussed in the next sub-section). At these locations, there is [[]]

]] between GNF-Ziron rods and the symmetric Zircaloy-2 rods. Both GNF-Ziron and Zircaloy-2 cladding exhibited some minor level of localized crud spalling (white patches) as shown in Figure 2-12. The spalling is not extensive and is primarily observed after brushing of the fuel rod prior to the visual inspection.

For the more recently initiated LUA program at Plant V, GNF-Ziron and Zircaloy-2 at [[]], Figure 2-11, which was predominantly due to crud build up, consistent with the plant water chemistry and measured profilometry. The measurements show that crud build up on cladding [[]]

]] In Figure 2-13, the visual appearances of GNF-Ziron and Zircaloy-2 cladding from symmetric locations in the same assembly are compared. The comparison is for locations away from spacers and shows that GNF-Ziron and Zircaloy-2 [[]] (Enhanced corrosion or shadow corrosion at spacer locations are discussed in the next sub-section).

The Plant G LUA also included GNF-Ziron as the water rod material. Following discharge at [[]] bundle average exposure, GNF-Ziron and Zircaloy-2 water rods were sent to the hot cell for destructive evaluation. The corrosion behavior in terms of the average inside diameter (ID), outside diameter (OD) and total oxide thickness at [[]] elevations is shown in Figure 2-14. The results show some axial variations in oxide thickness for both GNF-Ziron and Zircaloy-2. In this comparison, Zircaloy-2 appeared to undergo [[]]

]] On a rod average basis, the combined OD plus ID oxide thickness was [[]]

In summary, testing up to [[]] cycles in Plant K and inspections of LUAs in Plants G and V up to [[]] indicate GNF-Ziron and Zircaloy-2 have [[]]

2.4.2 Corrosion Benefit of GNF-Ziron: Under Enhanced Corrosion Conditions

[[]] performance of GNF-Ziron relative to Zircaloy-2 has been observed when: (i) under shadow corrosion conditions in BWRs and (ii) water chemistry has been deliberately adjusted in test reactors.

- (i) **Shadow Corrosion Related:** Near spacer locations, both GNF-Ziron and Zircaloy-2 show presence of enhanced (nodular) corrosion due to “shadow” effects associated with the Inconel spacer. The enhanced corrosion is commonly termed shadow corrosion because the corrosion enhancement on the zirconium alloy is related to the presence of a dissimilar metal, such as stainless steel or Inconel, and the area of enhanced corrosion often resembles the shape, or shadow, of the dissimilar metal. Shadow corrosion is particularly noticeable in the GNF2 and older GE12 fuel designs, for which the spacers are composed entirely of an Inconel alloy. In other fuel designs that use Zircaloy spacers with Inconel springs, the shadow corrosion affected smaller regions of the cladding in accordance with less Inconel material present.

A GNF-Ziron vs. Zircaloy-2 comparison of shadow corrosion due to spacer springs (alloy X750) from the LUA at Plant G after [] bundle average exposure is shown in Figure 2-15. [] shadow corrosion. The [] shadow corrosion is consistent with prior Zircaloy-2 spacers designs with Inconel springs. The visual comparison in Figure 2-15 does not provide information on the oxide thickness and []; both alloys exhibited minor levels of spalling.

Water rods of GNF-Ziron and Zircaloy-2 from the LUA program at Plant G after [] bundle average exposure have been examined in the hotcell. The spacer locations near the ~36-inch elevation were examined in more detail metallographically as shown in Figure 2-16. To aid the comparison, boxes are drawn on the macroscopic visual pictures in Figure 2-16 to indicate the expected contact region with the Inconel spring. Visually, a large difference between the two alloys [] Oxide thickness was measured in several (~12) locations evenly distributed around a quarter ring section of each water rod. Figure 2-16 shows the clear presence of enhanced corrosion typical of shadow corrosion for Zircaloy-2. []

]]

Further indication of [] was obtained from poolside inspection of a LUA at Plant V after [] bundle average exposure. Figure 2-17 shows a comparison of EC liftoff measurements at spacer locations from a pair of GNF-Ziron and Zircaloy-2 fuel rods that were placed in symmetric locations in the assembly. Both fuel rods showed appreciable crud deposition in the lower (~10 to 30-inch) elevations, which determined the values of maximum liftoff away from spacers shown in Figure 2-11 and discussed earlier. The measurements summarized in Figure 2-17 are obtained from [] pair of symmetric GNF-Ziron and Zircaloy-2 fuel rods characterized at [] intervals azimuthally as well as [] other pairs characterized at [] intervals. The focus in this discussion is the difference in the corrosion enhancement observed at spacer locations. Figure 2-17 shows that the shadow corrosion enhancement for GNF-Ziron []

]] as shown in

Figure 2-18. Figure 2-18 shows examples of enhanced shadow corrosion at fuel rod spacer locations for the GNF-Ziron and Zircaloy-2 pairs characterized in Figure 2-17 at different axial elevations. Each upper and lower pair represents a comparison at the same spacer location in fuel rods symmetrically located within the fuel assembly. Visual examinations show that, at Plant V, shadow corrosion on Zircaloy-2 generally manifests as [], which in some cases were []

]] GNF-Ziron in comparison generally exhibited [[
]] shadow corrosion.

While the exact mechanism for shadow corrosion remains the subject of on-going research, it should be noted that when the phenomenon was first observed, shadow corrosion was described as a form of nodular corrosion (Reference 2.4). [[

]]

- (ii) **Water Chemistry Effect:** The Halden BWR corrosion loop was used to conduct a series of tests in which the water chemistry was deliberately controlled and varied. The test condition simulated the thermo-hydraulic and nuclear conditions. The tested water chemistry included variations in the oxygen and hydrogen concentrations as well as additives such as Zn and sulfate. The detailed conditions are given in Table 2-1 and the test duration was [[]]. Post-irradiation metallographic examination showed that [[

]] Table 2-1 shows that [[

]]

**Table 2-1 Summary of Corrosion Oxide Thickness Test Results Performed in the BWR
Corrosion Loop of the Halden Test Reactor**

[[

]]

Figure 2-1 In-Reactor Operational Experience of GNF-Ziron

[[

]]

Figure 2-2 Hydrogen Content as a Function of Accumulated Fast Neutron Fluence

[[

]]

Figure 2-3 Corrosion Weight Gain as a Function of Accumulated Fast Neutron Fluence

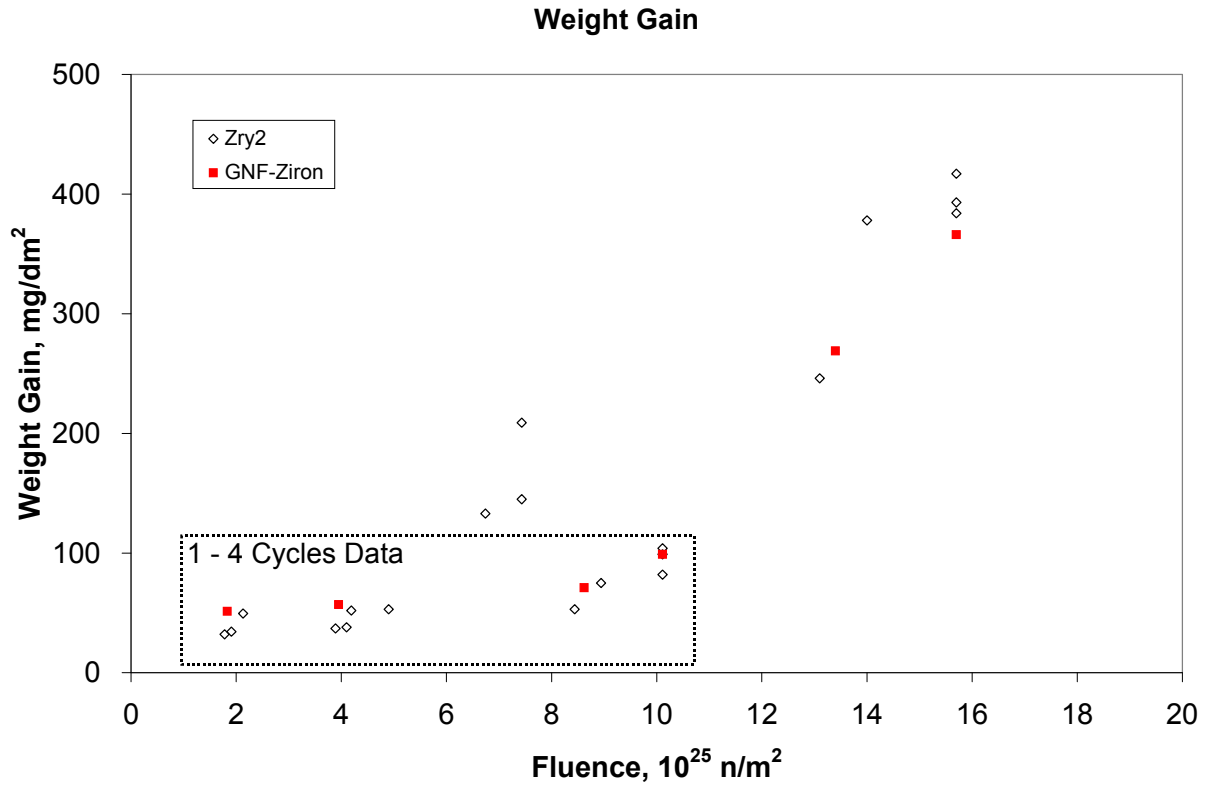


Figure 2-4 Hydrogen Concentration as a Function of Corrosion Weight Gain

[[

]]

Figure 2-5 Hydrogen Pickup as a Function of Accumulated Fast Neutron Fluence

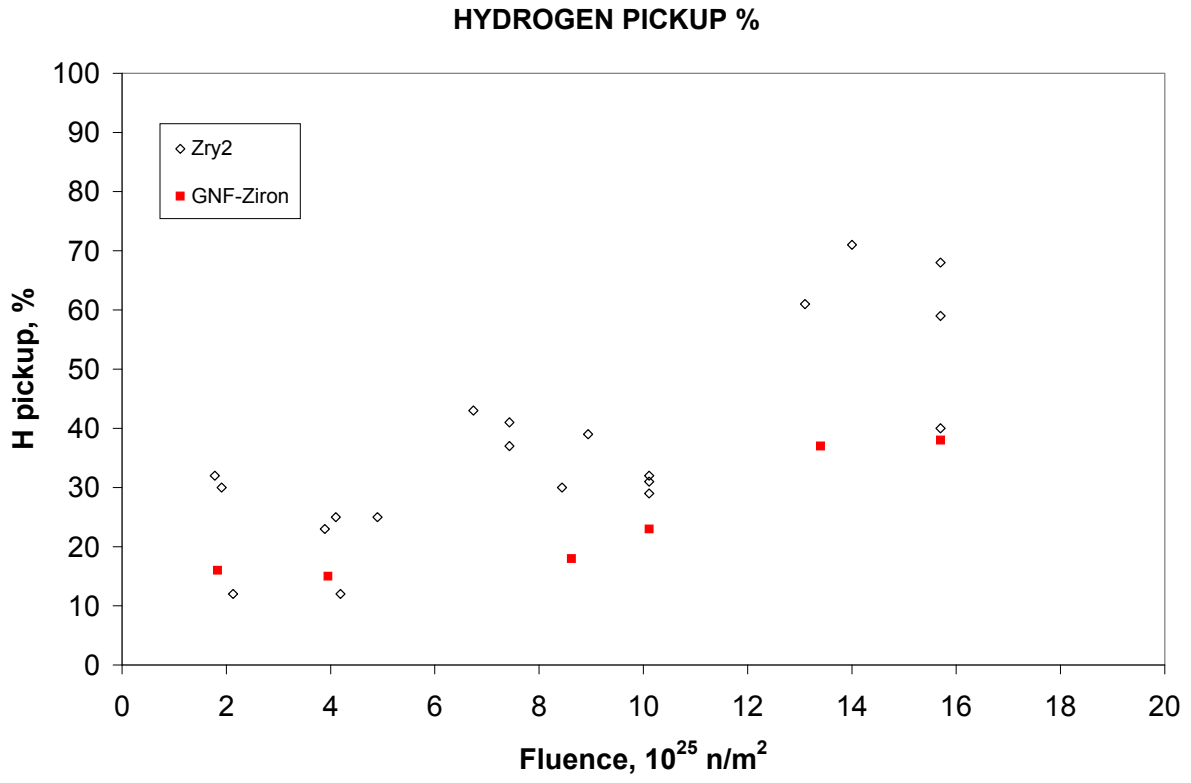


Figure 2-6 Hydrogen Concentration in Water Rods and Unfueled Cladding as a Function of Residence Time

[[

]]

Figure 2-7 Hydrogen Concentration in Fuel Cladding as a Function of Residence Time

[[

]]

Figure 2-8 Channel Shadow Corrosion Bow After 1 and 2 Cycles of Operation

[[

]]

Figure 2-9 Corrosion Weight Gain After 72 Hours Autoclave Testing at 400°C For Zircaloy-2 and GNF-Ziron as a Function of [[]]

[[

]]

Figure 2-10 Corrosion Weight Gain After Two-Step Test at 410°C /520°C for Zircaloy-2 and GNF-Ziron as a Function of [[]]

[[

]]

Figure 2-11 Poolside Eddy Current Liftoff from LUA Programs at Plant G And Plant V

[[

]]

Note: Maximum Effective Liftoff (MELO) represents the maximum of the running average over a 6-inch axial length.

**Figure 2-12 Comparison Of Visual Appearances of GNF-Ziron (Lower Row) And
Zircaloy-2 (Upper Row) Cladding Away from Spacer Locations after [[]]
Exposure (Plant G)**

[[

]]

**Figure 2-13 Comparison of Visual Appearances of GNF-Ziron (Lower Row) And
Zircaloy-2 (Upper Row) Cladding Away from Spacer Locations after [[]]
Exposure (Plant V)**

[[

]]

**Figure 2-14 Metallographic Oxide Thickness in GNF-Ziron And Zircaloy-2 Water Rods
after [] Bundle Average Exposure (Plant G)**

[

]

Figure 2-15 Comparison of Visual Appearances of GNF-Ziron (Lower Row) and Zircaloy-2 (Upper Row) Cladding at Spacer Locations at Similar Axial Elevations after [[]] Bundle Average Exposure (Plant G)

[[

]]

Figure 2-16 Visual Appearance Water Rod Made from GNF-Ziron (Right and Zircaloy-2 (Left) at a Spacer Location (~36 Inch Elevation) after [] Bundle Average Exposure (Plant G)

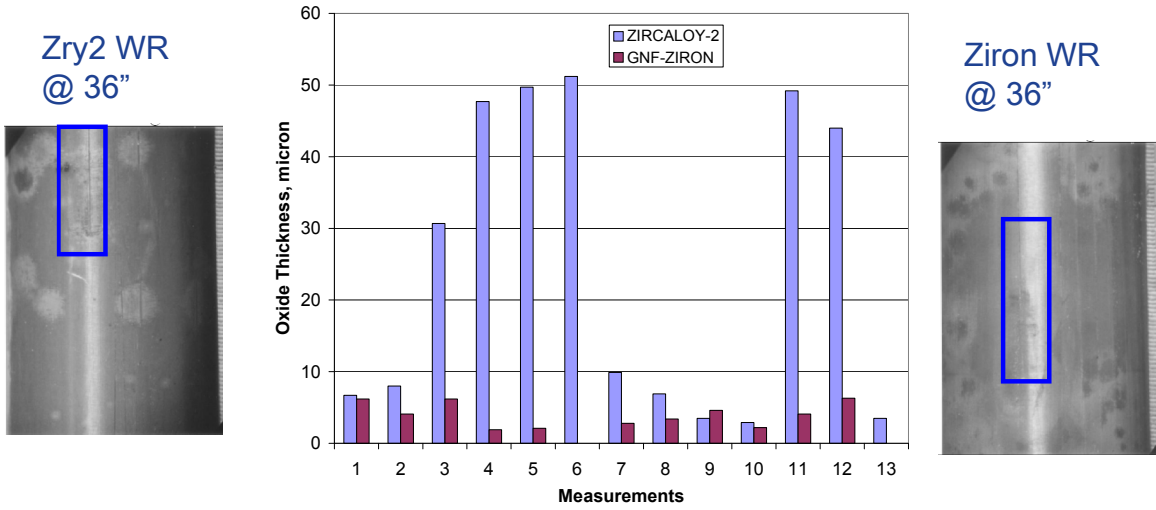
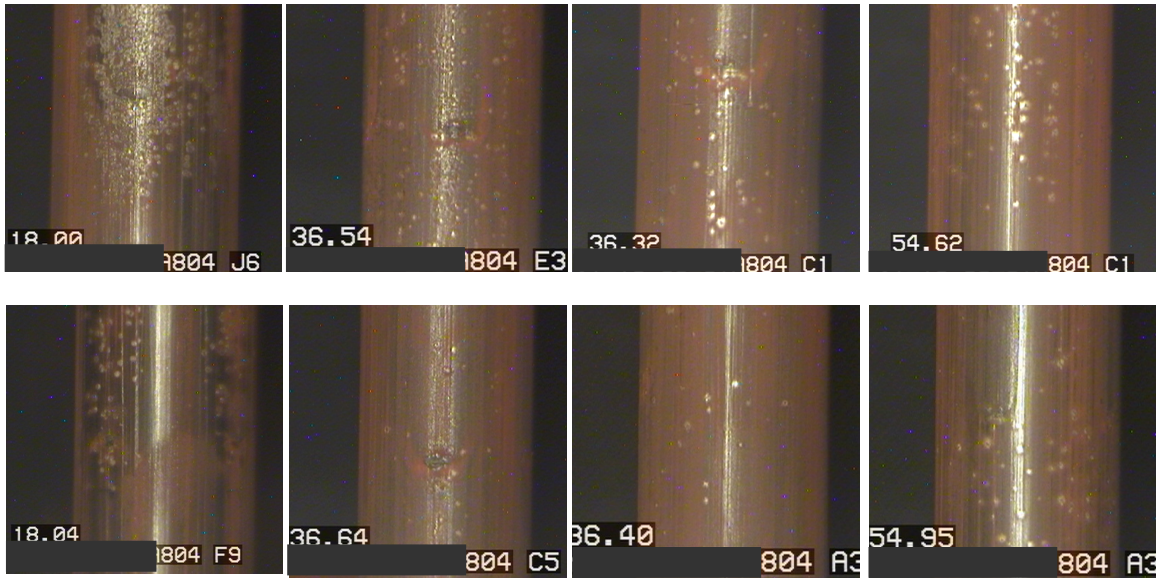


Figure 2-17 Comparison of Eddy Current Lutoff Measurements at Spacer Locations

[[

]]

Figure 2-18 Comparison of Visual Appearances of GNF-Ziron (Lower Row) and Zircaloy-2 (Upper Row) Cladding at Spacer Locations at Same Axial Elevation after ~15 GWd/MTU Exposure (Plant V)



3.0 Methods and Licensing Assessment

This section reviews the criteria for demonstrating compliance to GNF fuel design licensing criteria, including compliance to NRC approved methodologies. For convenience, the licensing assessment is divided in three major groups: compliance to fuel design licensing criteria; compliance for the nuclear-thermal-hydraulic analyses that are performed with the GNF core simulator; and compliance for the thermal-mechanical analyses that are more closely linked to the material performance of a new alloy such as GNF-Ziron.

3.1 Fuel Design Licensing

GNF licenses fuel designs with the NRC based on specific analyses performed in accordance with the fuel licensing acceptance criteria as specified in GESTAR II (Reference 1.1). The fuel licensing acceptance criteria included in GESTAR II establishes the basis for evaluating new fuel designs, developing the critical power correlation for these designs, and determining the applicability of generic analyses to these new designs. Compliance with the fuel licensing acceptance criteria constitutes NRC acceptance of the fuel design without specific NRC review.

The GESTAR II licensing criteria are applicable to fuel design licensing but not necessarily adequate to determine the licensing requirements of a component material. The application of GNF-Ziron as a component material within a specific fuel design will require revision of the appropriate compliance report. In this regard, this document provides justification that GNF-Ziron is capable of meeting current licensing acceptance criteria per GESTAR II. Incorporation of GNF-Ziron into GNF fuel designs would occur on a component-by-component basis by providing appropriate analyses supporting an amendment to the GNF compliance reports for a specific fuel design. Where specific NRC regulations limit application of GNF-Ziron, such as 10 CFR 50.46 Appendix K, GNF will provide justification and request an exemption prior to first application of the material in a plant.

3.2 Nuclear & Thermal/Hydraulic Methods

GNF methodologies are, in general, not dependent on composition of the fuel lattice, except for the maximum enrichment of Uranium and Gadolinia in the fuel pellets. The introduction of GNF-Ziron as a material for cladding and channels does not require a change to the approved nuclear and thermal hydraulic methodologies. However, there are GNF-Ziron properties that are briefly addressed in this section due to their relative importance within GNF's methodologies. They are the thermal conductivity, heat capacity, neutron absorption, irradiation growth and hydrogen absorption. The first two parameters, thermal conductivity and heat capacity, are discussed in Appendix B where it is concluded that these properties are [[

]]

The third parameter, neutron absorption, will address the effect of relative changes in the composition [[]] between GNF-Ziron and Zircaloy 2. Using thermal neutron activation microscopic cross sections and the isotopic and compositional abundance in the alloy, an estimation of the macroscopic cross section can be obtained. The relative change in macroscopic cross section of Zirconium in GNF-Ziron is [[

]]

The remaining parameters, irradiation growth and hydrogen absorption, may influence the predicted component distortion or component material properties resulting in increased uncertainties in the nuclear and thermal-hydraulic methodologies. These parameters have been discussed in Appendix B and Section 2.3 respectively. In Appendix B, it was concluded that GNF-Ziron and Zircaloy 2 have [[]] In Section 2.3, it was concluded that [[

]]

To continue with the licensing assessment, the thermal-mechanical parameters that were identified as relevant to the GNF methodologies are discussed in detail in Section 3.3.

3.3 Thermal/Mechanical Methods

A primary GNF fuel rod design objective is to preclude systematic defects arising under the conditions of authorized operation including normal steady-state operation and anticipated operational occurrences (AOOs). This fuel rod design objective is achieved by the imposition of mechanistic limits on the predicted performance of the fuel under the conditions of authorized operation. The GNF fuel rod thermal-mechanical performance model PRIME (Reference 3.1) is applied to provide conservative fuel performance predictions for comparison against the specified performance limits. The material properties of the fuel cladding used in thermal-mechanical design and licensing analyses include:

1. Elastic properties (elastic modulus and Poisson's ratio),
2. Thermal expansion coefficients,
3. Plastic properties (yield and ultimate stress and failure strain),
4. Creep properties,
5. Fatigue properties,
6. Irradiation growth properties, and
7. Corrosion properties.

The elastic properties and thermal expansion coefficients are only weakly dependent upon alloy composition and more dependent upon fabrication process, specifically the reduction process and the resulting texture. Because [[

]] and thus on the thermal-mechanical performance of fuel rods. Likewise, the plastic, creep, fatigue and irradiation growth properties are also only weakly dependent upon alloy composition. However, these properties are strongly dependent upon the fabrication process, specifically the final heat treatment. Because [[

]]

Finally, [[

]] In addition to the fuel rod model, a set of design criteria, defined in Table 3-1, are applied in the fuel rod thermal-mechanical design process to ensure that fuel rod mechanical integrity is maintained throughout the fuel rod design lifetime. An assessment of the effect of GNF-Ziron cladding on each of these design and licensing criteria, along with the applicability of the PRIME models and associated uncertainties, is presented below.

3.3.1 Fuel Rod Internal Pressure

The design and licensing limit on fuel rod internal pressure is that it cannot exceed the value for which the cladding creepout rate becomes equal to the fuel pellet fission product solid swelling rate. If the fuel rod internal pressure exceeds the coolant pressure, the resulting cladding tensile hoop stress causes the cladding to deform outward (cladding creepout). If the rate of cladding outward deformation exceeds irradiation swelling rate of the fuel pellet, the pellet-cladding gap will begin to open. An increase in the pellet-cladding gap would reduce the pellet-cladding thermal conductance and thereby increase the fuel temperature. The increased fuel temperature would result in further fuel pellet fission gas release, greater fuel rod internal pressure, and, correspondingly, a faster rate of cladding outward deformation and gap opening. A limit on fuel rod internal pressure is applied to prevent this adverse feedback condition.

Conformance to the fuel rod internal pressure design and licensing criterion is performed through the evaluation of a fuel rod internal pressure design ratio, defined as

$$\text{Design Ratio} = \frac{\text{Fuel Rod Internal pressure}}{\text{Fuel Rod Critical pressure}}$$

where the fuel rod critical pressure corresponds to the pressure that would cause the fuel rod cladding to creep out at a rate equal to the instantaneous fuel pellet irradiation swelling rate. The design ratio is evaluated statistically and formulated in such a way that a value of 1.0 provides 95% probability at 95% confidence level that the fuel rod internal pressure will not exceed the critical pressure. Therefore, the value of the fuel rod internal pressure design ratio is required to be < 1.0.

Key cladding properties/phenomena that may affect the compliance with the fuel rod internal pressure limits are cladding creep, conductivity, thermal expansion, and cladding oxidation. Based on the available in-reactor creep test data, as shown in Appendix B (Figure B-10), [[

]] and no adverse effect on fuel rod internal pressure design ratio calculations is expected due to the use of GNF-Ziron rather than Zircaloy-2 cladding.

3.3.2 Fuel Melting

The design and licensing limit on fuel temperature is that the maximum fuel centerline temperature cannot exceed the fuel melting temperature during normal operation, including anticipated operational occurrences. This fuel temperature limit is applied to preclude any sudden shifting of molten fuel in the interior of the fuel rods, and any subsequent potential cladding damage.

The PRIME03 application methodology determines a thermal overpower criterion, in terms of linear heat generation rate (LHGR), as the maximum power to assure with 95% probability at 95% confidence that fuel melting will not occur. Cladding corrosion performance has the potential of affecting fuel melt margin. If the cladding is oxidized at a faster rate than assumed in the thermal-mechanical analysis, then the thicker oxide layer at the cladding outer surface will increase the resistance to heat transfer from the cladding to the coolant. As a consequence, the fuel temperature will be higher and the margin to fuel melting will be lower than predicted. [[

]] with no adverse effect on calculated margin to fuel melting due to the use of GNF-Ziron rather than Zircaloy-2 cladding.

3.3.3 Cladding Strain

The licensing limit for cladding strain requires the [[

]]. These limits are applied to ensure that fuel rod failure due to pellet-cladding mechanical interaction will not occur.

Like the thermal overpower criterion, a mechanical overpower criterion is defined to assure the [[]] limit is not exceeded. This overpower criterion is based upon the calculated cladding strain at the most limiting exposure and is applied to ensure that the calculated strain is less than the strain limit. All evaluations for cladding strain are performed using a worst-tolerance basis for fuel rod design parameters, as opposed to the statistical procedure used for other criteria. It is noted that the [[

]], as shown in Appendix B. Moreover, cladding ductility is a function of fluence and hydrogen content and, as shown in Section 2.3, [[

]] Thus it is concluded there will be no adverse effect on calculated margin to the cladding strain limit due to the use of GNF-Ziron rather than Zircaloy-2 cladding.

3.3.4 Cladding Stress/Strain

The fuel assembly components are evaluated to ensure that the fuel will not fail due to stresses or strains exceeding the mechanical capability of the components. The fuel rod stress analysis is performed using a Monte Carlo statistical method to calculate the effects of pressure differential, cladding ovality, radial thermal gradients, spacer contact, thermal bow and circumferential thermal gradients. The calculated stresses are compared with the appropriate design limits to produce a design ratio. Design ratios of less than 1.0 provide 95% probability at 95% confidence that the fuel will not fail due to stresses or strains exceeding the fuel assembly component mechanical capability.

As reported in Appendix B, [[

]]

Therefore, no adverse effect on margins to cladding stress/strain limits is expected due to the use of GNF-Ziron rather than Zircaloy-2 cladding.

3.3.5 Cladding Fatigue

Fuel rod cladding is evaluated to ensure that strains due to cyclic loadings will not exceed the fatigue capability of the cladding material. The cladding strain cycles are analyzed using the rain flow cycle counting method. The fractional fatigue life expended for each strain cycle is determined and summed over the total number of cycles to determine the total fatigue life expended over the fuel design lifetime. The calculated upper 95% total fatigue life expended is required to be <1.0 to provide adequate assurance that the fuel will not fail due to fatigue.

Appendix B.3.e shows [[

]] Therefore, for fuel with

GNF-Ziron cladding, loss of mechanical integrity due to cladding fatigue is not expected.

3.3.6 Cladding Creep Collapse

The fuel rod is evaluated in accordance with Reference 3.2 to assure that fuel rod failure as a result of cladding collapse into a fuel column axial gap will not occur. Such collapse occurs due to a slow increase of cladding initial ovality caused by creep from the combined effect of reactor coolant pressure, temperature and fast neutron flux on the cladding over the axial gap. This condition occurs at cladding stress levels far below that required for elastic buckling or plastic deformation. As noted above, [[]] Thus, it can be concluded that failure due to cladding creep collapse is not expected for fuel rods with GNF-Ziron cladding.

3.3.7 Postulated Loss-of-Coolant Accident

3.3.7.1 Current Criteria

10 CFR Part 50.46, "Acceptance criteria for emergency core cooling systems for light-water nuclear power reactors," requires that the calculated emergency core cooling system (ECCS) performance for reactors with Zircaloy or ZIRLO fuel cladding meet certain criteria. 10 CFR Part 50 Appendix K, "ECCS Evaluation Models," further requires that the Baker-Just (BJ) equation be used in the ECCS evaluation model to determine the rate of energy release, cladding oxidation, and hydrogen generation after a postulated loss-of-coolant accident (LOCA). The BJ equation presumes the use of Zircaloy or ZIRLO fuel cladding. The composition of GNF-Ziron is outside of the composition range defined in ASTM industry standards for Zircalloys. Because there is no provision for cladding material other than Zircaloy or ZIRLO in 10 CFR 50.46 and Part 50 Appendix K, the use of GNF-Ziron as the cladding material will therefore require exemptions to the current 10 CFR 50.46 and Part 50 Appendix K.

10 CFR 50.46 has requirements related to the maximum cladding oxidation, peak cladding temperature, maximum hydrogen generation, coolable geometry and long-term cooling. High temperature oxidation tests have been conducted on GNF-Ziron as discussed in Appendix B.5. Specifically, the oxidation kinetics data at 1000°C (1273 K) and 1200°C (1473 K) shown in Appendix B, Figures B-13 and B-14, show the oxidation data for GNF-Ziron [[]]

At these temperatures, the BJ relationship generally predicts more oxidation than the CP relationship. Therefore, the use of the BJ equation remains conservative in the postulated LOCA circumstances relative to the measured GNF-Ziron data.

The maximum cladding oxidation and peak cladding temperature limits are collectively known as the embrittlement criteria. In order to address the potential embrittlement due to cladding oxidation associated with a postulated LOCA, ring compression tests were conducted to determine the post-test ductility following oxidation at 1000°C and 1200°C. The resultant post-quench ductilities (based on offset strain) as a function of Equivalent Cladding Reacted (ECR) shown in Appendix B, Figures B-16 and B-17, show that the embrittlement ECR is compliant with the current 17% ECR criterion. It should be noted that the ECR values in Figures B-16 and B-17 are expressed using the CP correlation, whereas the current embrittlement criterion is based on the BJ equation. If the BJ equation were used, the embrittlement ductility

for GNF-Ziron would be higher than indicated in Figures B-16 and B-17 (based on offset strain) or in Figures B-18 and B-19 (based on permanent strain). The test results thus indicate margin to embrittlement relative to the current 17% ECR cladding oxidation limit stated in 10 CFR 50.46. As discussed in Section B.5.b, additional quench tests under a restraining load have been conducted. The test results showed ductility up to [] ECR based on BJ. Although these tests differ from the ring-compression testing that forms the basis of the post-quench ductility criteria in 10 CFR 50.46, these results provide additional assurance that adequate post-quench ductility in the GNF-Ziron cladding material will be maintained.

The []

[]

A comparison of test data obtained from GNF-Ziron with available data for Zircaloy is shown in Figure B-6, which shows that the high temperature perforation characteristics for GNF-Ziron []

[]

The high temperature test results described above thus demonstrate in that the requirements currently in 10 CFR 50.46 and Part 50 Appendix K can be met using GNF-Ziron as the cladding material. There is no anticipated decrease in coolability or increase in dose consequences as a result of a postulated LOCA for GNF-Ziron relative to evaluations performed assuming Zircaloy cladding.

3.3.7.2 Likely Future Criteria

The NRC is currently in the process of revising 10 CFR 50.46(b), as communicated in Reference 3.3. The specific details of the revision have not been finalized. The likely key changes are the change to a set of non-alloy-specific performance-based criteria, use of CP equation for ECR evaluation, addressing the potential for breakaway oxidation, setting of

hydrogen (exposure) dependent ECR limit, and accounting for oxidation on cladding inner surface in high exposure fuel.

The change to performance-based criteria will allow alloys such as GNF-Ziron to be more readily introduced as fuel cladding material. The high temperature oxidation characteristics compared with BJ and CP predictions are shown in Figures B-13 to B-15 and it is evident that the CP equation provides a better representation for GNF-Ziron behavior than BJ. The consistency of these doubled-sided oxidation results between GNF-Ziron and Zircaloy-2 imply that the inclusion of double-sided oxidation to account for inner surface oxidation in high exposure fuel would have the same applicability for the two alloys. The high temperature oxidation tests also serve the purpose of assessing the breakaway oxidation behavior. The results (Figures B-13 and B-15) confirm that breakaway oxidation at 1000°C had not occurred up to 5000 seconds, the longest time investigated and of interest for postulated LOCA considerations. The post-quench ductility data, shown in Figures B-16 to B-19, show that GNF-Ziron meets the CP-based 17% ECR embrittlement criterion (based on either 2% offset strain or 1% permanent strain) in the as-fabricated state. With respect to the hydrogen dependent ECR limit after irradiation, the data generated in Reference 3.4 from various irradiated Zr-based cladding alloys are expected to be applicable to GNF-Ziron (and Zircaloy-2), as the results reflect a generic, alloy independent hydrogen effect. In Figure 2-7, the hydrogen content in Zircaloy-2 cladding is shown as function of residence time. In the [] time frame, cladding hydrogen data obtained from fuel assemblies with between [] bundle average exposure typically showed []

[] of the fuel rod. Up to these levels of hydrogen, Figures 236 and 237 in Reference 3.4 show that []]. The data in Figure 2-7 specific to GNF-Ziron were obtained after [] bundle average exposure and []]. It is possible that []

]]

Although the revision to 10 CFR 50.46(b) is not yet complete, the high temperature test results described above thus demonstrate with a high degree of confidence that the requirements likely to be in the revised 10 CFR 50.46 would be met when GNF-Ziron is used as the cladding material.

3.3.8 Reactivity Insertion Accident

Current criteria related to the reactivity insertion accident (RIA) have limits that address radiological consequences due to fuel cladding failure and core coolability. Current criteria to prevent cladding failure for Control Rod Drop Accident (CRDA) for BWRs are: (a) radial average fuel enthalpy less than 170 cal/g at zero or low power, and (b) local heat flux below fuel thermal design limits for at-power events. Current criteria for core coolability are: (a) fuel radial average energy density not exceeding 280 cal/g, and (b) reactor pressure limited to be less than that causing stresses to exceed Service Level C of ASME Boiler and Pressure Vessel code. A

revision to the RIA criteria is currently in progress and an interim acceptance criterion for RIA has been issued (Reference 3.5). The interim criteria addressing cladding failure are:

- a) For zero power conditions, peak radial average fuel enthalpy greater than 170 cal/g for fuel rods with an internal rod pressure at or below system pressure and 150 cal/g for fuel rods with an internal rod pressure exceeding system pressure; for intermediate and full power conditions, fuel cladding is assumed to be failed if local heat flux exceeds thermal design limits and
- b) For BWRs, radial average fuel enthalpy greater than the hydrogen-dependent limits, in which the limiting radial average fuel enthalpy is lowered from 150 cal/g at 75 ppm hydrogen in cladding to 60 cal/g at 150 ppm hydrogen and greater.

For core coolability, the interim criteria are:

- a) Peak radial average fuel enthalpy must remain below 230 cal/g,
- b) Peak fuel temperature must remain below incipient fuel melting conditions,
- c) Mechanical energy generated as a result of (a) non-molten fuel-to-coolant interaction and (b) fuel rod burst must be addressed with respect to reactor pressure boundary, reactor internals, and fuel assembly structural integrity, and
- d) No loss of coolable geometry due to (a) fuel pellet and cladding fragmentation and dispersal and (b) fuel rod ballooning.

The current criteria are addressed through core design and energy deposition calculations. There is no requirement for specific inputs for cladding type or properties. It is understood that mechanical properties of the cladding have been embodied within the enthalpy-based criteria. Because the mechanical properties of GNF-Ziron [[]] Zircaloy-2 (Section B.3), the [[]]

Therefore, GNF-Ziron cladding complies with current criteria by following the same energy deposition based approach to core design.

The interim criteria introduce a failure criterion that is dependent on the hydrogen content of the cladding. The criterion itself is not alloy specific because for the RIA scenario the failure mechanism is dominated by effects associated with hydrogen. In other words, the response of different Zr-based cladding alloys is taken to be dependent on the hydrogen content rather than mechanical properties of each alloy. GNF-Ziron can therefore meet the same hydrogen content-based failure criteria in the same manner as Zircaloy-2. The corrosion and hydriding characteristics that lead up to hydrogen accumulation in the cladding are discussed in Section 2.4 and the mechanical properties are discussed in Appendix B.

4.0 Mechanical Design Assessment

In this section, the effect of applying GNF-Ziron material to GNF fuel bundle components is evaluated with respect to GNF's fuel bundle mechanical design bases. All fuel bundle components that are currently made of Zircaloy-2 (or Zircaloy-4) material may potentially be made from GNF-Ziron material. This list of components includes fuel rod cladding, water rods, fuel spacers, channels, and end plugs.

The effects on fuel rod thermal-mechanical licensing methodologies are discussed in Section 3.3. Additional evaluations performed as part of the fuel bundle mechanical design basis for the fuel rod as well as other Zircaloy components are shown in Table 4-1. Although not directly addressed in Section 3.3 or Table 4-1, high resistance to fretting (both with and without debris) is a key feature of GNF fuel assemblies. The resistance is achieved by including assembly design features to minimize fretting wear on the fuel rods at spacer contact points and to minimize ingress of debris in conjunction with the inherent fretting resistance of GNF cladding. The fretting resistance of the cladding depends upon the elastic properties of the material, including the hardness. As noted in Section 3.3 and Appendix B, these properties are only weakly dependent upon alloy composition but strongly dependent upon fabrication process, specifically the final heat treatment. Because [[

]]

In summary, the GNF-Ziron properties that are of primary importance in assessing the adequacy of the fuel bundle mechanical design are: elastic properties (Young's Modulus, Poisson's Ratio), thermal expansion, thinning due to corrosion, tensile strength (yield and ultimate), creep properties, fatigue and stress rupture life, crack growth rate and thresholds, irradiation growth, and hydrogen uptake. As discussed in Section 2.1, the material properties of GNF-Ziron are [[

]] There are no negative effects to the mechanical design bases for GNF fuel from changing bundle components from a Zircaloy-2 material to GNF-Ziron. Therefore, whether or not a fuel component is important to safety, it follows that all fuel components that are currently made from Zircaloy-2 may be changed to GNF-Ziron [[

]]

Table 4-1 Considerations for Supplementary Zircaloy Mechanical Design Bases

Primary Consideration	Material Properties used in the Design Basis Analysis	Additional Considerations
Fuel rod mechanical loads from internal pressure, spacer contact force, end plug fit up & weld	Young's Modulus, Yield Strength, Ultimate Strength, Poisson's Ratio, Thermal Expansion Coefficient, Fatigue Curve	Thinning due to corrosion, Weldability
Bundle differential component growth	Thermal Expansion Coefficient, Young's Modulus, Stress/Strain relationship, Creep Properties,	Irradiation induced growth, Hydrogen due to corrosion
Fuel rod spacing	Young's Modulus, Thermal Expansion Coefficient, Creep Properties	Irradiation induced growth
Spacer mechanical adequacy	Young's Modulus, Ultimate Strength, Fatigue Curve	Thinning due to corrosion, Hydrogen due to corrosion, Weldability
Water rod shipping, handling and bounding seismic event	Young's Modulus, Stress/Strain relationship, Fatigue Curve	
Channel pressure loads, distortion, bounding seismic event	Young's Modulus, Stress/Strain relationship, Creep Properties, Fatigue Curve, Stress Rupture Life	Irradiation induced growth, Hydrogen due to corrosion, Weldability
Component crack propagation analysis	Young's Modulus	Crack growth threshold and rates
Component ductility	Stress/Strain Relationship	Hydrogen due to corrosion

5.0 Summary

GNF began research and development of GNF-Ziron for use in fuel designs during the 1980s. This report summarizes the characterization of GNF-Ziron based on 20+ years of experience, which includes (as applicable) material performance characterization of unirradiated and irradiated material, test reactors and commercial reactor operations, post-irradiation testing, and material coupons as well as commercial fuel assemblies and fuel components. The results from this experience base have been used to demonstrate that GNF-Ziron has essentially [[

]]

Section 2.0 and Appendices A and B of this report evaluate the effect of the compositional changes relative to metallurgical and material processing. These evaluations concluded that the [[

]] as well. Therefore, GNF-Ziron is [[
]]

Appendix B to this report evaluates the material performance characteristics of GNF-Ziron relative to the physical, thermal and mechanical material characteristics used within GNF's design basis methodologies. Those evaluations demonstrate that GNF-Ziron is [[

]] Section 3.0 of this report evaluates the characteristics shown in the Appendix relative to the NRC-approved methodologies licensed per GESTAR II, to conclude that GNF's approved methods remain applicable to, and unaffected by, incorporation of GNF-Ziron. Section 4.0 of this report evaluates the mechanical design bases used for GNF fuel designs, where the relevant material properties used in the analyses have been assessed against those described in the Appendix to show the mechanical design bases for GNF fuel designs would remain unaffected by incorporation of GNF-Ziron.

Section 3.3.7 and 3.3.8 in this report assesses the effect of GNF-Ziron on postulated LOCA and RIA conditions. Per the LOCA criteria outlined in 10 CFR 50.46 high temperature oxidation tests have been conducted on GNF-Ziron which indicate margin to embrittlement relative to the current 17% ECR cladding oxidation limit stated in 10 CFR 50.46. Proposed changes to the LOCA regulatory criteria indicate a change to performance-based criteria. GNF-Ziron will provide additional margin relative to Zircaloy-2 [[

]]

Related to RIA criteria, the compliance to the current regulatory criteria is demonstrated through core design and is not necessarily a fuel cladding material criteria. However, the interim criteria introduce failure criteria that are dependent on the hydrogen content of the cladding. Because GNF-Ziron mechanical properties [[

]]

This report concludes that GNF-Ziron is capable of meeting all current design and licensing criteria as well as proposed criteria. No safety concerns have been identified as a result of the proposed change from Zircaloy-2 (or Zircaloy-4) to GNF-Ziron for GNF fuel components. Acceptance of this report by the NRC results in GNF-Ziron being considered an “approved” material. GNF will incorporate the safety evaluation report from the NRC into GESTAR II, reflecting that GNF-Ziron is approved for use in GNF fuel bundle components and cladding. Incorporation within GNF fuel designs will require an Amendment 22 compliance report. The current wording and interpretation of the criteria in 10 CFR 50.46 and Part 50 Appendix K requires an exemption for GNF-Ziron prior to use in a given plant.

6.0 References

- 1.1 Global Nuclear Fuel, “General Electric Standard Application for Reactor Fuel,” NEDE-24011-P-A-17 and NEDE-24011-P-A-17-US, September 2010.
- 2.1 [[

]]
- 2.2 [[

]]
- 2.3 [[

]]
- 2.4 [[

]]
- 3.1 Global Nuclear Fuel, “The PRIME Model for Analysis of Fuel Rod Thermal-Mechanical Performance,” Technical Bases - NEDC-33256P-A, Revision 1, Qualification – NEDC-33257P-A, Revision 1, and Application Methodology - NEDC-33258P-A, Revision 1, September 2010.
- 3.2 GE Hitachi Nuclear Energy, “Cladding Creep Collapse,” NEDC-33139P-A, July 2005.
- 3.3 Advance Notice of Proposed Rulemaking, 10 CFR Part 50, “Performance-Based Emergency Core Cooling System Acceptance Criteria,” Federal Register Volume 74, Number 155, 2009.
- 3.4 NUREG/CR-6967, ANL-07/04, “Cladding Embrittlement During Postulated Loss-of-Coolant Accidents,” July 2008.
- 3.5 NUREG-0800, “Fuel System Design,” Revision 3, March 2007.

Table A-1 GNF Alloy Chemical Composition for GNF-Ziron and Zircaloy

Element	Zircaloy-2 (Per ASTM B350 [*])	Zircaloy-4 (Per ASTM B350 [*])	GNF-Ziron
	wt %		
Sn	1.20-1.70	1.20-1.70	[[]]
Fe	0.07-0.20	0.18-0.24	[[]]
Cr	0.05-0.15	0.07-0.13	[[]]
Ni	0.03-0.08	-	[[]]
Fe+Cr+Ni	0.18-0.38	-	-
O (Oxygen)	0.09-0.15	0.09-0.15	[[]]
Zr	Balance	Balance	Balance
Total Alloy ^{**}	1.47-2.23	1.54-2.22	[[]]

Notes:

* Except for O

** Includes O

A.2 Material Processing

[[

]]

A.3 Basic Metallurgical Characteristics

A.3.a Grain Structure and Size

GNF-Ziron, and Zircaloy-2, components deployed in GNF's fuel designs are [[

]], as discussed in Section A.1.

Figure A-1 Examples of GNF-Ziron (left) and Zircaloy-2 (right) in Cladding of Ziron

[[

]]

A.3.b Texture

As shown in Table A-1, the composition of GNF-Ziron is predominantly zirconium, as is Zircaloy-2. The crystal structure of both alloys is hexagonally close packed at temperatures below the $\alpha/\alpha+\beta$ transition temperature (~865°C, 1590°F). In polycrystalline zirconium alloys, the distribution of basal planes is generally non-uniform in space. The proportion of a particular crystal plane relative to three orthogonal reference directions is often expressed in terms of a set of Kearns' F factors. The plane of most interest is the basal plane and the three reference directions are typically the longitudinal, the transverse (or circumferential), and the radial directions for cladding; for channel strips, the third reference direction is the thickness direction of the strip. The F factors for the three reference directions are usually written as the F_l , F_t and F_r . The three F parameters in essence describe the crystallographic texture of the alloy. The texture of the alloy can affect properties; for example, the axial elongation due to irradiation growth of cladding is dependent on the F_l factor for the basal plane.

The texture of zirconium alloys is dependent on the reduction/rolling schedule and on the annealing condition. [[

]] Figure A-2 provides a GNF-Ziron versus Zircaloy-2 comparison of the basal plane F factors for cladding and channel materials that have been produced under the same reduction or rolling sequence and annealing conditions. The results show that there are differences in the texture of cladding compared with channel material; for example, the F_l values for cladding are [[]] than that for channel, and F_t values for cladding are [[]] than that for channel. The difference is consistent with the differences in the reduction sequence for cladding and rolling for channel material. The texture data shown in Figure A-2 shows that for a given process/anneal sequence, [[

]] between the two alloys.

**Figure A-2 Comparison of Texture in GNF-Ziron and Zircaloy-2 10x10 Cladding
(Upper) and Channel Strip (Lower)**

[[

]]

A.3.c Second Phase Particles

In addition to grain structure and texture, another important attribute of zirconium alloys used in light water reactor fuel components is the dispersion of SPPs. The SPPs are formed because the solubility for alloying elements such as Fe, Cr and Ni is very low below the solvus temperature of approximately 850°C. The distribution of the SPPs affects primarily the corrosion characteristics of the zirconium alloy. The formation and growth of SPPs are dependent on the thermal treatment history, and the SPP distribution is set by the coarsening time below the solvus temperature. Typically, the SPP distribution can be controlled separately from grain size or

texture, because recrystallization and texture development can occur at significantly lower temperatures than the SPP solvus temperature.

As discussed previously, GNF offers GNF-Ziron and Zircaloy-2 cladding [[

]]
 A comparison of SPPs in GNF-Ziron and Zircaloy-2 [[]] observed in a transmission electron microscope (TEM) are provided in Figure A-3. The measured SPP statistics are given in Table A-2. It should be noted that TEM examinations and SPP measurements are conducted for the purpose of obtaining a better representative description of the cladding type and are not meant to show compliance with any SPP size requirement. The results are considered typical [[

]] of the alloy. However, there appears to be [[

]] from TEM examinations.

The [[

]], GNF-Ziron cladding, like Zircaloy-2, possesses adequate performance under BWR conditions. The in-reactor corrosion behavior of GNF-Ziron is discussed in Section 2.0 of this document. SPP size and distribution are not expected to affect the high temperature oxidation behavior because the SPPs dissolve rapidly once the solvus temperature is exceeded.

During in-reactor operation, the neutron flux induces dissolution of the SPPs. The result is a decrease in the number density of the SPPs and the SPPs can become completely dissolved at sufficiently high fluences or irradiation times, both dependent on the initial SPP size. The dissolution process in effect releases the alloying elements in the SPPs into the surrounding matrix. The SPPs formed in GNF-Ziron and Zircaloy-2 are $Zr(Fe,Cr)_2$ and $Zr_2(Fe,Ni)$. The dissolution processes for the two types of SPPs are different. For the $Zr(Fe,Cr)_2$ SPPs, the dissolution rate of Fe is faster than that of Cr resulting in the SPP becoming enriched in Cr as the SPP dissolves. The Cr is eventually released from any Cr enriched SPPs or remnants. In contrast, $Zr_2(Fe,Ni)$ SPPs appear to dissolve without appreciable change in the Fe/Ni ratio. Figure A-4 shows representative data on the Fe/(Fe+Cr) and Fe/(Fe+Ni) ratios for $Zr(Fe,Cr)_2$ and $Zr_2(Fe,Ni)$, respectively, in GNF-Ziron and Zircaloy-2 as a function of irradiation time. In the unirradiated condition, Figure A-4 shows that the [[

]]. Figure A-4 also shows that the evolution of SPP composition is [[

]]

Table A-2 Comparison of Outer Surface SPP Size in GNF-Ziron and Zircaloy-2 Cladding [[]]

[[

]]

Figure A-3 TEM Micrograph Showing SPPs in [[

]]

[[

]]

Figure A-4 Changes in Fe Content in $Zr(Fe,Cr)_2$ and $Zr_2(Fe,Ni)$ SPPs in GNF-Ziron and Zircaloy-2

[[

]]

APPENDIX B

B. Material Properties Assessment Physical Properties

B.1 Physical Properties

B.1.a Metal Properties

The material density and melting point are characteristics considered within approved methods to license fuel. These characteristics are [[

]] The values provided in References 1 and 2 for both Zircaloy-2 and Zircaloy-4 are, [[

]] In principle, variations are expected if chemical composition variations are significant. A single density value is typically given for Zircaloy-2 and Zircaloy-4 in References 1 and 2. This is because the compositional differences between Zircaloy-2 and Zircaloy-4, and composition variations within the specification of each Zircaloy, are not appreciable enough to cause significant variation in the density. The alloying elements Sn, Fe, Cr and Ni can all have an effect of decreasing the melting temperature of zirconium if the compositional change is large. In contrast, oxygen has the effect of increasing the melting temperature. In Reference 2, the effect due to oxygen is specifically addressed; however, [[

]] In Reference 2, the variation in melting point due to compositional variations in Zircaloy-2 and Zircaloy-4 is typically addressed through a 20°C uncertainty. As discussed in Section A.1, the [[

]]

B.1.b Oxide Properties

Zirconium Oxide forms on the exposed surfaces of Zirconium alloys when operated in the BWR reactor. The oxide density is a characteristic considered within approved methods to license fuel. This characteristic is [[

]] A single density value is typically given for ZrO_2 regardless of whether the base material is Zircaloy-2 or Zircaloy-4 (Reference 2). This is because the compositional differences between Zircaloy-2 and Zircaloy-4, and composition variations within the specification of each Zircaloy, are not appreciable enough to cause significant changes in the oxide properties. As discussed in Section A.1, the [[

]]

B.2 Thermal Properties

Table B-1 lists thermal properties [[

]] These properties are not sensitive to small changes in composition, such that Zircaloy-2 and Zircaloy-4 are generally treated without differentiation. However, specific heat, thermal conductance and thermal expansion can be composition dependent if the compositional change is large. [[

]]

As noted in Reference 2, the thermal conductivity is primarily a function of temperature. Other material characteristics, such as residual stress levels, crystal orientation, and minor composition differences may have a secondary influence on thermal conductivity. In this context, the compositional difference between Zircaloy-2 and Zircaloy-4 is not considered significant. In Figure B-1, the thermal conductivity of GNF-Ziron as a function of temperature is shown. [[

]]

The design bases for these properties are experimental correlations developed in Reference 2. [[

]]

Table B-1 Thermal Properties of GNF-Ziron Unaffected by Composition Difference Between GNF-Ziron and Zircaloy

[[
]]

Figure B-1 Comparison of Thermal Conductivity of GNF-Ziron with Reference Zircaloy-2 as a Function of Temperature

[[

]]

B.2.a Oxide Properties

The specific heat and thermal conductivity of the oxide are characteristics considered within approved methods to license fuel. As discussed in Section B.1.b, these characteristics are [[

]]

In general, the thermal properties of the oxide are more sensitive to the condition and structure, which are heavily influenced by operational considerations, rather than any minor elemental compositions within the oxide crystal lattice. A single specific heat value is typically given for ZrO_2 regardless of whether the base material is Zircaloy-2 or Zircaloy-4 (Reference 2). Similarly, thermal conductivity values are typically provided based on the structure of the corrosion film over a broad range of temperatures. This is because the compositional differences between Zircaloy-2 and Zircaloy-4, and composition variations within the specification of each Zircaloy, are not appreciable enough to cause significant changes in the oxide properties. As discussed in Section A.1, the [[

]]

B.3 Mechanical Properties

B.3.a Modulus and Poisson's Ratio

Young's modulus and shear modulus are properties that are sensitive to temperature. Young's modulus and shear modulus are also sensitive to directionality due to the presence of texture in anisotropic Zr-based alloys. Poisson's ratio is generally not strongly sensitive to the temperature and texture typical of Zr-based alloys used as fuel components, and a constant value is given in Reference 2. A differentiation of these properties based on the exact composition of the Zircalloys is generally not warranted. [[

]]

B.3.b Tensile Properties

Yield and Ultimate Stress

In considering the plastic deformation behavior of Zircalloys and similar alloys, the stress-strain relationship is strongly influenced by temperature and fast neutron fluence. As temperature increases, the yield and ultimate tensile stresses generally decrease, while the ductility increases. As fast neutron fluence increases, the yield and ultimate tensile stresses generally increase, while the ductility decreases. The irradiation hardening occurs rapidly with fast neutron fluence and generally saturate at about $3.5 \times 10^{25} \text{ n/m}^2$.

In the unirradiated condition, a number of factors potentially could affect the tensile properties. These include oxygen and tin content and manufacturing related factors such as texture and level of cold work. A range in tensile properties is, therefore, expected when measurements are taken from several production lots. The composition, other than oxygen and tin, of Zircalloy is generally not a primary factor, such that, for example, a differentiation is not made between Zircaloy-2 and Zircaloy-4 in Reference 2. In Figure B-2, measured tensile properties taken from GNF-Ziron cladding used in the 1999 and the more recent LUA programs are compared with a set of measurements from Zircaloy-2 cladding taken over a similar range of production period. The measurements were made in accordance with ASTM E8 "Standard Test Methods for Tension Testing of Metallic Materials" for testing at ambient temperature and ASTM E21 "Standard Test Methods for Elevated Temperature Tension Tests of Metallic Materials" for testing at elevated temperatures (ETs). As shown in Figure B-2, [[

]]

Tensile properties of irradiated GNF-Ziron were assessed using mini-tensile specimens irradiated in Plant C and the ATR in the US and somewhat larger specimens irradiated in Plant K in Japan. The ATR irradiations were carried out at a nominal irradiation temperature of 300°C with an uncertainty of ±25°C. These specimens were discharged at fluences of [[

]]. Companion Zircaloy-2 specimens were irradiated and discharged at fluences of [[]]. Following irradiation in the ATR, tensile tests were conducted at 300°C. Tests following irradiation in Plant K (for up to 6 cycles of operation) were carried out at 23°C, 288°C and 343°C (300K, 561K and 616K). The highest fast neutron fluence reached was about $15 \times 10^{25} \text{ n/m}^2$. The mechanical properties obtained from these tests are shown in Figure B-3 to Figure B-5. From Figure B-3 and Figure B-4, it can be seen that the unirradiated strength values are all higher compared with the unirradiated strength values shown Figure B-2. This difference could be due to differences in detailed manufacturing methods. Also, the strengths of GNF-Ziron tested at room temperature (RT) appear to be higher compared with Zircaloy-2 in Figure B-3 and Figure B-4. This difference is likely due to the [[

]] Zircaloy-2. The main purpose of Figure B-3 and Figure B-4 is to show the variation in strengths due to irradiation. [[

]] For fuel component mechanical designs, the design criteria are generally based on minimum strength requirements. [[

]]

Figure B-2 Yield Strength, Ultimate Tensile Strength and Elongation at Room Temperature and at 343°C Elevated Temperature for GNF-Ziron and Zircaloy-2

[[

]]

Figure B-3 Yield Strength as a Function of Fluence at Room and Elevated Temperatures

[[

]]

Figure B-4 Ultimate Tensile Strength as a Function of Fluence at Room and Elevated Temperatures

[[

]]

Figure B-5 Total Elongation as a Function of Fluence at Room and Elevated Temperatures

[[

]]

Strain

In the unirradiated condition the elongation data shown in Figure B-2 show [[

]]

Degradation in tensile strain bearing capability of cladding is of interest under a number of steady state and design-basis accident conditions. As shown in Figure B-5, there is little

difference in the degradation of irradiation embrittlement in the [[

]]

B.3.c Perforation Stress

A correlation relating the perforation temperature for Zircaloy fuel clad under internal pressure and rapid heating conditions is currently used to assess the cladding integrity during transient events. Such a correlation is typically presented as a function of engineering hoop stress for heating rates less than 5.5°C/sec in the temperature range 650 - 1540°C. Burst tests were conducted on GNF-Ziron with target burst pressures between [[]] at a heating rate of [[]]. Figure B-6 shows the data for GNF-Ziron compared with literature data for Zircaloy obtained for a range of heating rates (Reference 3). For clarity, only correlation lines for three heating rates are shown in Figure B-6. [[

]]

Figure B-6 High Temperature Burst Test Data for GNF-Ziron Compared with Zircaloy Correlation Lines for Different Heating Rates (Reference 3)

[[

]]

B.3.d Hardness

Hardness data is used to characterize attributes associated with fuel/cladding contact on the inner cladding surface of the fuel rod. Hardness is a measure of the resistance of material to plastic deformation and is dependent on tensile properties of the material as well as how the hardness test is conducted. Figure B-7 provides the performance of GNF-Ziron relative to Zircaloy-2 following irradiation in Plant K and a commercial power reactor. [[

]]

Figure B-7 Hardness as a Function of Fluence

[[

]]

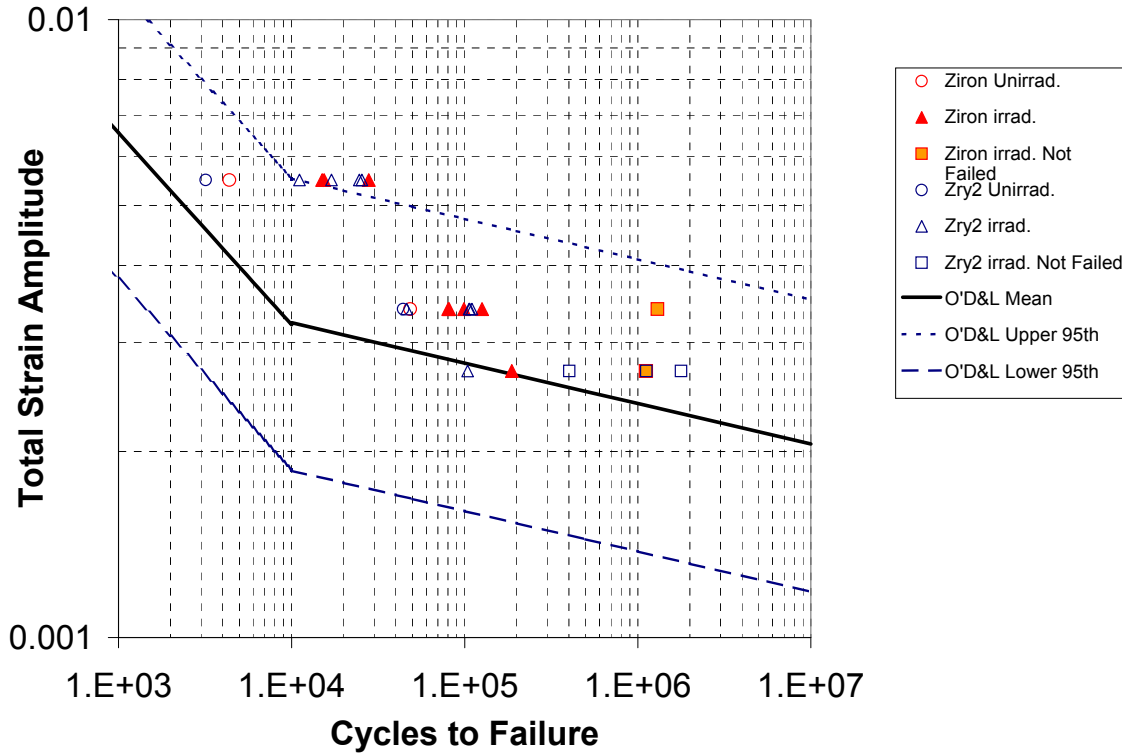
B.3.e Fatigue

For the temperature range of interest to BWR applications (260 to 320°C) the cyclic stress-strain behavior of Zircalloys is related to their respective monotonic stress-strain behavior resulting from cyclic hardening and softening. Available data, Reference 2, for Zircalloys does not indicate sensitivity to the composition of Zircaloy-2 or Zircaloy-4. The data can be described

using $E = bN^k$ relationship; generally two relationships are used, one for low cycle and one for high cycles to failure. Fatigue testing has been conducted on GNF-Ziron and Zircaloy-2 following up to 6 cycles of irradiation in Plant K. The data are presented in Figure B-8. [[

]]

Figure B-8 Cyclic Strain Amplitude as a Function of Cycles



B.3.f Creep

Creep is dependent on the stress history of the cladding wall, as induced by the internal gas pressure, the coolant pressure, and the fuel cladding mechanical contact forces, as well as the temperature and irradiation histories. [[

]]

In the irradiation program at Plant K, creep specimens of GNF-Ziron, and Zircaloy-2 for comparison, pressured to 150 MPa were assessed for creep strain after 1, 2 4 and 6 cycles of irradiation at ~560K. The results are shown in Figure B-9 as a function of fast neutron fluence ($E > 1\text{MeV}$). [[

]]

For Zircaloys, it is established that creep strain is dependent on fast neutron flux in the low stress regime and at the Plant K irradiation

temperature. [[

]]

Figure B-9 Creep Strain of GNF-Ziron and Zircaloy-2 as a Function of Fast Fluence

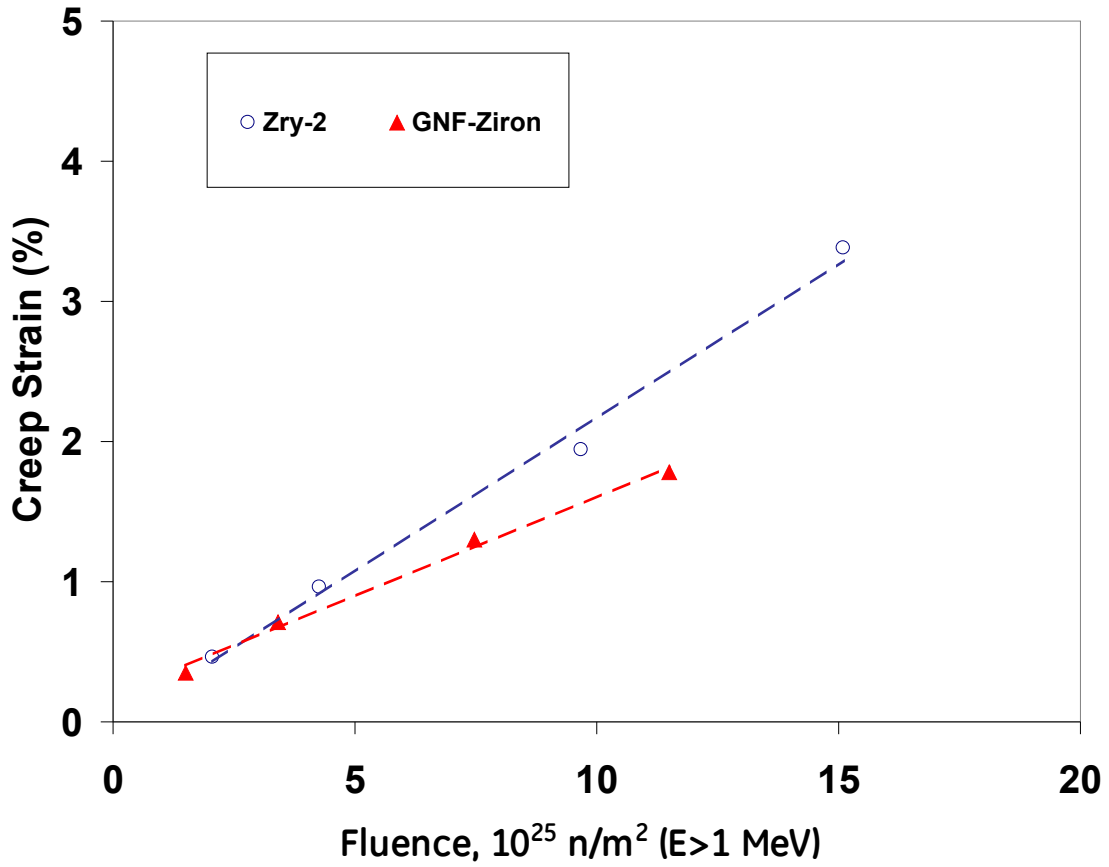


Figure B-10 Adjusted Creep Strain as a Function of Fluence for GNF-Ziron and Zircaloy-2

[[

]]

B.4 Irradiation Growth

Previous measurements of GNF-Ziron spacer strip coupons irradiated in the ATR reactor up to a fluence level of about 6×10^{25} n/m² have shown a similar growth behavior as Zircaloy-2. In order to confirm the similarity in growth behavior at higher fluence levels, in-reactor tests were conducted in the BOR-60 test reactor. The fast neutron fluence level reached was [[]] ($E > 1 \text{ MeV}$). Because the energy spectrum in the BOR-60 reactor is different than in typical BWRs, the corresponding fast neutron fluence for BWR is numerically ~30% greater. For the irradiation growth testing program at BOR-60, specimens of production cladding and channel strip of GNF-Ziron and reference Zircaloy-2 were pre-characterized for texture, specifically the Kern F-factor for basal planes. The pre-characterization of texture is important as the growth of zirconium alloys is texture dependent and is related the basal F-factor for the direction of interest through a (1-3 F) term. The specimens were pre-oxidized as a measure to prevent hydrogenation of the specimens from the sodium coolant during irradiation. The growth measurements are therefore unaffected by potential contributions from hydriding. The irradiation growth results from the BOR-60 reactor are shown in Figure B-11. The data

presented in Figure B-11 have been adjusted by normalizing to a basal F-factor [] in the longitudinal direction. With this normalization, a more meaningful comparison of the irradiation growth behavior of the alloys can be made without texture effect, as indicated by the consistency between cladding and channel materials that have different measured F-factors. The results show that up to [] in equivalent BWR fluence ($\sim 11 \times 10^{25}$ n/m² in BOR-60), [] At higher fluence levels, GNF-Ziron [] The results suggest [] in terms of equivalent BWR fast neutron fluence or [] in terms of equivalent burnup.

Irradiation growth behavior can also be deduced from growth measurements made on fuel assembly components, such as water rods, although in these cases, other factors such as hydriding resulting from corrosion could contribute to the measured growth. In the LUA program at Plant G, length measurements of GNF-Ziron and Zircaloy-2 water rods were taken at high exposures. The results are shown in Figure B-12 together with other data for Zircaloy-2 water rods at high exposures. A direct comparison is possible at [] when both GNF-Ziron and Zircaloy-2 water rods irradiated at Plant G were measured. Both water rods are subject to contribution from hydriding due to corrosion. However, the average hydrogen concentrations measured [] Despite the potential contribution from hydriding, the measured growth in GNF-Ziron is [] and is consistent with the BOR-60 irradiation growth results shown in Figure B-11. The difference in water rod growth behavior between the two alloys []

Figure B-11 Irradiation Growth of Cladding and Strip Specimens of GNF-Ziron and Zircaloy-2 Irradiated in the BOR-60 Reactor

[[

]]

Note: The plotted data have been adjusted to a common texture [[]] and are shown as function of equivalent fast neutron fluence ($E > 1$ MeV) for the BWR at 40% void fraction.

Figure B-12 Comparison of Water Rod Growth of GNF-Ziron with Zircaloy-2

[[

]]

B.5 High Temperature Behavior

B.5.a High Temperature Oxidation Kinetics

Oxidation kinetics under simulated LOCA conditions have been obtained for GNF-Ziron. The high temperature oxidation tests were conducted at 1000 and 1200°C (1273 and 1473K) steam. Two sets of data have been acquired for GNF-Ziron, one of which was conducted by the ANL. The resultant data are shown in Figure B-13 and Figure B-14. At 1000°C, Figure B-13, the weight gain results from both sets of tests are lower than expected based on the CP relationship. At 1200°C, Figure B-14, the weight gain results from both sets of tests are more closely matched to the expected CP relationship. Figure B-13 and Figure B-14 show that there appears to be differences between the results obtained by the two laboratories. One likely reason could be due to whether transient time during heat up is accounted for; the heat up transient time was accounted for by one of the two laboratories in accordance with method described in Reference 7. [[

]]

In a recent investigation on high temperature oxidation, conducted at ANL (Reference 7), it was noted that the phenomenon of breakaway oxidation could be an additional mechanism for causing cladding embrittlement during postulated loss-of-coolant accidents conditions. The

breakaway oxidation occurs when the oxidation kinetics accelerates relative to the diffusion control oxidation mechanism that is the underlying assumption for BJ and CP relationships. Breakaway oxidation can lead to significantly increased hydrogen absorption by the cladding and result in cladding embrittlement. The net result is that the time to reach a particular percentage of ECR could be shorter than BJ and CP predictions, and the resultant cladding embrittlement could be greater than expected based on BJ and CP relationships. The time to breakaway oxidation for a given alloy is dependent on the oxidation temperature. For most zirconium-based alloys, the shortest time before onset of breakaway oxidation occurs around 1000°C. However, the time to the onset of breakaway oxidation is alloy dependent. For the purpose of considering cladding embrittlement due to this effect, a time of greater than 5000 seconds before the onset of breakaway oxidation is considered to be very long (Reference 7). The comparisons of oxidation kinetics GNF-Ziron at 1000°C with that predicted by the BJ and CP relationships is shown in Figure B-15. From Figure B-15, it can be seen that GNF-Ziron did not exhibit breakaway oxidation at 1000°C up to 5000 seconds. The behavior of GNF-Ziron to breakaway oxidation at 1000°C is consistent with the behavior of Zircaloy-2 as reported in Reference 7.

B.5.b Post-Quench Ductility

Two sets of data have been acquired for GNF-Ziron. The first set was obtained at ANL using the same methodology as used in Reference 7. In the ANL work, ring compression testing was used to determine the post-test ductility at RT for 1000°C-oxidized rings and at 135°C for 1200°C-oxidized rings. Following oxidation at both temperatures the oxidized specimen was quenched at 800°C. The purpose for conducting these tests is to determine the level of oxidation at which the cladding becomes brittle. For ring compression tests, the criterion for embrittlement used in Reference 7 for various Zr-based alloys including Zircaloy-2 was 2% offset strain, and in Reference 8 is 1% permanent strain. The same criteria are used here for discussion regarding GNF-Ziron. For cladding currently used in commercial light water reactors, the embrittling oxidation level is typically greater than 15% ECR (Reference 7). The results for offset strains versus ECR (based on CP) for GNF-Ziron together with data for Zircaloy-2 and Zircaloy-4 reported in Reference 8 are shown in Figure B-16 for 1000°C-oxidized samples and in Figure B-17 for 1200°C-oxidized samples. The results based on permanent strains are shown in Figure B-18 for 1000°C-oxidized samples and in Figure B-19 for 1200°C-oxidized samples. Two samples were tested at each oxidation level. For oxidation at 1000°C, GNF-Ziron was tested after oxidizing to four ECR levels. The results, Figure B-16 and Figure B-18 show that GNF-Ziron exhibited ductility greater than the embrittlement criteria at room temperature for ECR (CP) [[]], which is the limit of testing. For oxidation at 1200°C, post-quench ductility testing was performed at three ECR levels. The results, Figure B-17 and Figure B-19, show that both Ziron samples exhibited ductility ([[]]) greater than the embrittlement criteria at 135°C for 17% ECR (CP). [[]]

]] Figure B-17 and Figure B-19 show that at 17% ECR, [[]]

]] ([[]]

)). The ductile-to-brittle transition ECR (CP) for Zircaloy-2 was deduced to be about [[]] based on testing that included 20% ECR. [[

]]

In addition to ring compression testing conducted at ANL, additional testing under a restraining load were conducted at ~1100°C and ~1200°C, with cladding oxidized to [[]] ECR (BJ) at ~1100°C and to [[]] ECR at ~1200°C. The results showed that cladding oxidized to [[]] ECR and less did not fail and that only the cladding oxidized to [[]] ECR failed.

Figure B-13 Comparison of Weight Gain for GNF-Ziron and Zircaloy-2 at 1000°C

[[

]]

Figure B-14 Comparison of Weight Gain for GNF-Ziron and Zircaloy-2 at 1200°C

[[

]]

Figure B-15 Comparison of Weight Gain for GNF-Ziron at 1000°C with Baker-Just and Cathcart-Pawel Relationships

[[

]]

Figure B-16 Post-Quench Ductility (Offset Strain) at Room Temperature for GNF-Ziron and Zircaloy-2 as a Function of ECR at 1000°C Followed by Quench from 800°C

[[

]]

Figure B-17 Post-Quench Ductility (Offset Strain) at 135°C for GNF-Ziron and Zircaloy-2 as a Function of ECR at 1200°C Followed by Quench from 800°C

[[

]]

Figure B-18 Post-Quench Ductility (Permanent Strain) at Room Temperature for GNF-Ziron and Zircaloy-2 as a Function of ECR at 1000°C Followed by Quench from 800°C

[[

]]

Figure B-19 Post-Quench Ductility (Permanent Strain) at 135°C for GNF-Ziron and Zircaloy-2 as a Function of ECR at 1200°C Followed by Quench from 800°C

[[

]]

APPENDIX C

C. References for Appendices

1. B. Lustman and F. Kerze Jr., The Metallurgy of Zirconium, McGraw-Hill, 1955.
2. SCDAP/RELAP5/MOD3.1 Code Manual Volume IV: MATPRO -- A Library of Materials Properties for Light-Water-Reactor Accident Analysis, NUREG/CR-6150, EGG-2720 Volume IV, 1993.
3. NUREG-0630, "Cladding Swelling and Rupture Models for LOCA Analysis."
4. W. J. O'Donnell, B. F. Langer, "Fatigue Design Basis for Zircaloy Components," Nuclear Science Engineering, 20, 1, (1964).
5. Letter from C. O. Thomas (NRC) to J. S. Charnley (GE), "Acceptance for Referencing of Licensing Topical Report NEDE-24011-P-A Amendment 7 to Revision 6, GE Standard Application for Reactor Fuel," March 1, 1985.
6. Global Nuclear Fuel, "The PRIME Model for Analysis of Fuel Rod Thermal – Mechanical Performance, Part 1 – Technical Bases," NEDC-33256P-A, Revision 1, September 2010.
7. NUREG/CR-6967, ANL-07/04, "Cladding Embrittlement During Postulated Loss-of-Coolant Accidents."
8. Advance Notice of Proposed Rulemaking, 10 CFR Part 50, "Performance-Based Emergency Core Cooling System Acceptance Criteria," Federal Register Volume 74, Number. 155, 2009.